Macromolecules

Article

pubs.acs.org/Macromolecules

Intertwined Lamello-Columnar Coassemblies in Liquid-Crystalline Side-Chain π-Conjugated Polymers: Toward a New Class of Nanostructured Supramolecular Organic Semiconductors

Danli Zeng,[†] Ibtissam Tahar-Djebbar,[†] Yiming Xiao,[†] Farid Kameche,[†] Navaphun Kayunkid,[‡] Martin Brinkmann,[‡] Daniel Guillon,[§] Benoît Heinrich,[§] Bertrand Donnio,[§,⊥,*] Dimitri A. Ivanov,[∥] Emmanuelle Lacaze,[○] David Kreher,[†] Fabrice Mathevet,[†,*] and André-Jean Attias[†,*]

[†]Laboratoire de Chimie des Polymères (LCP), UMR 7610 CNRS-Université Pierre et Marie Curie Paris 6, 3 Rue Galilée, 94200 Ivry-sur-Seine, France

[‡]Institut Charles Sadron (ICS), UPR 22 (CNRS), 23 rue du Loess, BP 84047, 67034 Strasbourg cedex 2, France

[§]Institut de Physique et Chimie des Matériaux de Strasbourg (IPCMS), UMR 7504, CNRS-Université de Strasbourg, 23 rue du Loess, 67034 Strasbourg Cedex 2, France

[⊥]Complex Assemblies of Soft Matter Laboratory (COMPASS), UMI 3254, CNRS-Rhodia/Solvay—University of Pennsylvania, CRTB, 350 George Patterson Boulevard, Bristol, Pennsylvania 19007, United States

[∥]Institut de Science des Matériaux de Mulhouse (IS2M), UMR 7361, CNRS-Université de Haute Alsace, 15, rue Jean Starcky, BP 2488, 68057 Mulhouse cedex, France

[○]Institut des NanoSciences de Paris (INSP), UMR 7588, CNRS-Université Pierre et Marie Curie Paris 6, 4 Place Jussieu, 75252 Paris Cedex 05, France

Supporting Information

ABSTRACT: A set of liquid-crystalline polymeric systems, associating at once the regioregular polythiophene backbone and pending mesogenic triphenylenes, is reported. Two series, namely regular homopolymers and alternating copolymers, were prepared by adapting a Grignard metathesis-based methodology, allowing some of the relevant structural parameters to be sequentially and independently modified. The thermal and self-organization behaviors of these uncommon macromolecular systems were investigated by polarized-light optical microscopy, differential scanning calorimetry and temperature-dependent small-angle X-ray scattering. Most polymers self-organize into mesophases possessing intertwined lamello-columnar morphologies, resulting from the simultaneous coexistence of lamellar and columnar sublattices. The successful preparation of oriented thin films of several of these polymeric homologues allowed further investigations by atomic force microscopy, transmission electron microscopy, electron diffraction, and grazing-incidence SAXS, which provided a deeper insight of the intricate supramolecular organizational modes, including the complete elucidation of the structure of the lamello-columnar mesophases. This simple and versatile strategy provides a route to elaborate polymeric materials incorporating two intercalated separate pathways toward charge carrier transport, of paramount importance for future electronic and optoelectronic applications.

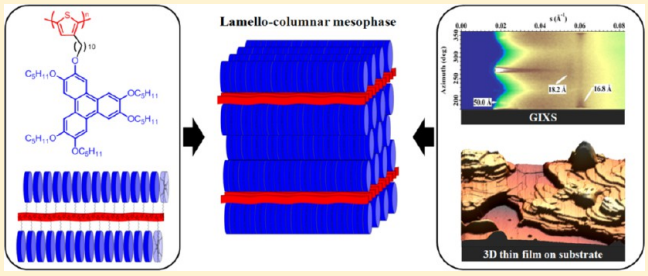

INTRODUCTION

The control of the nanoscale morphology of π-conjugated polymeric architectures, providing long-range order, and the establishment of reliable structure-properties relationships remain the major and fundamental issues in the field of organic semiconductors in view of developing and fabricating light-weight, flexible, low-cost and high-performance organic devices.[1] Substantial advances have been accomplished[2,3] since the discovery of electronic conductivity in π-conjugated polymers,[4,5] and current efforts focus essentially on two conceptually different approaches either based on the elaboration of conjugated block copolymers, where each block acts as different type of electro-active carriers,[6] or alternatively on liquid-crystalline π-conjugated polymers, bearing side-on conjugated mesogenic groups.[7] The former class of materials takes advantage of the block copolymers ability for phase separation into well-ordered spherical, cylindrical, or lamellar morphologies with periodicities ranging in the nanometers scale. Since such periodicities are commensurate with exciton diffusion lengths, the two latter

Received: October 2, 2013
Revised: February 1, 2014
Published: February 24, 2014

   dx.doi.org/10.1021/ma4020356 | Macromolecules 2014, 47, 1715−1731

morphologies are of particular interest for photovoltaic devices based on bulk heterojunctions thin films.[8] Indeed, these morphologies offer the possibility to form separate conduction pathways for charge carriers, thanks to the antagonistic chemical nature of each block leading to nanosegregation. However, optimal charge transport properties would require enhancing the segregation to form long-range correlated structures with acute orientation control of the regular pathway alternation. This goal is difficult to achieve by tuning the block structures and lengths but can be more easily envisaged with a liquid-crystalline polymeric architecture. Liquid crystals are indeed outstanding examples of soft self-assemblies that combine order and fluidity, within components self-organizing into a wide diversity of long-range ordered, periodic structures.[9,10] In addition, liquid crystal assemblies can form thin films which are intrinsically self-healing since structural defects are corrected automatically during the process of self-assembly, and whose morphology can be controlled at the molecular level. Last but not the least, the large variety of avaliable mesogenic architectures that could be combined to π-conjugated backbones should allow the acurate tuning of the electronic and transport properties of the material by controlling the chain microstructure at the molecular level as well.

However, careful and systematic investigations of the relationships between liquid-crystalline conjugated polymer structure, and nano- and macroscopic ordering are less commonly encountered.[7] Their elucidation is crucial for designing optimized liquid-crystalline conjugated polymeric architectures in order to enhance the electronic performances of the ultimate organic devices, but only a few recent reports have focused on the synthesis of new conjugated polymeric architectures. A remarkable features shared by the "semi-rigid" linear π-conjugated polymers known to date[11] (see for example, polyacetylenes (**PA**), polyanilines (**PANI**), polycarbazoles (**PC**), polypyrroles (**PPy**), polythiophenes (**PT**), poly(*p*-phenylenevinylene)s (**PPV**), poly(p-phenylene)s (**PPP**), poly(phenyleneethynylene)s (**PPE**), polyfluorenes (**PF**), and their mixed copolymeric derivatives, to cite but a few) is that the presence of just "non-innocent", inert pending alkyl chains along the backbone already produces drastic properties changes: not only it enhances their solubility in classical solvents and/or decreases their melting temperatures, but also it improves the backbone microsegregation which often gives rise to lamellae of well-registered linear polymeric backbones, over rather long persistence lengths.[12,13] Concomitantly, the electronic performances may occasionally be considerably altered with respect to the nonsubstituted ones by several orders of magnitude, essentially due to distortions of the rigid backbone and local interruptions of the π-conjugation along the chain. In such respects, the most promising types of liquid crystal-based conjugated polymers giving the best compromise are those based on thiophene-backbones, particularly the regioregular poly(3-alkylthiophene)s being the benchmark architecture.[14] A fortiori, it may be anticipated that the lateral grafting of various functional groups with stronger segregating abilities such as for example fluorinated chains[15] or mesogenic moieties[7] may further favor their self-organization into low-dimensional liquid-crystalline structures, in a similar way as the more conventional side-chain liquid-crystalline polymers.[16] By a judicious design, the properties of regularly alternating domains of conjugated polymeric backbones and functional conjugated mesogenic moieties can be adjusted independently by the functions born by the individual molecular fragments, e.g., electronic affinities, n- or p-type carriers, and the morphology of the self-assemblies (e.g., films). Consequently, side-chain liquid-crystalline π-conjugated polymers (SCLCCP) may also offer the opportunity to form two separate pathways for charge transport carriers, as previously mentioned for conjugated block copolymers. Besides this strategy, it has been shown that liquid-crystalline character can also be induced by incorporating more rigid segments in the polymer backbone, as for example poly(2,5-bis(3-alkylthiophen-2-yl)thieno[3,2-*b*]thiophene (PBTTT) systems.[3a]

Up to now, side-chain liquid-crystalline π-conjugated polymers have been studied in order to induce some anisotropy to the semiconducting backbones, and mainly calamitic side-mesogens have been utilized to induce mesomorphism.[7] This archetypical molecular structure gives rise to original supramolecular smectic-like organizations consisting of two distinct, regularly alternated subdomains that involve two-dimensional (2D) thin sheets associated with the lateral stack of the backbones and sublayers formed by the lateral registry of the calamitic mesogens; these sublayers are further separated by an aliphatic medium.[17] Alternatively, side groups liquid-crystalline π-conjugated polymers involving discotic[18] or tappered[19] mesogens would provide an interesting variant of this architecture as the mesogen stacking into columns is well-known to produce efficient one-dimensional (1D) conductive pathway.[20] However, so far except few attempts,[18,19] no SCLCCP architecture has been reported to combine within one single bulk material intercalated lamellar and columnar sublayers capable of potential simultaneous 1D and 2D electronic transport. Obviously, besides trivial considerations related to restrictions upon respective fragment sizes and chemical incompatibilities, such a condition appears hardly to be fulfilled when combining fragments giving rise simultaneously to both 1D- and 2D-organizations, respectively. This is obvious for low-molecular weight compounds associating calamitic and discotic mesogens, which were found to lead exclusively to lamellar mesophases with short-range correlated stacking of the discotic moieties.[21−23] For shape-persistent, π-conjugated polymers, however, the registered sublayers containing the polymeric backbones intrinsically confer in-plane ordering and one intuitively can foresee that this will help long-range columnar ordering persistence beyond the intercalated polymer sublayers. In this context, we previously reported the first lamello-columnar mesophase formation of a liquid-crystalline π-conjugated polythiophene.[24] In this preliminary study, a new regioregular poly(3-decylthiophene) polymer postfunctionalized with side-on discotic triphenylene moieties was synthesized, and the supramolecular self-organization into a peculiar lamello-columnar mesophase where a 2D oblique columnar lattice and the lamellar piling coexisted in the same structure was deduced from SAXS measurements. The respective orientations of both lattices could however not be determined at this stage, precluding the complete mesophase structure characterization.

Here, we report a comprehensive study, exploring systematically the relationships between polymeric architecture and nano- and macroscale organizations, of thin films of SCLCCP in order to develop new insights into the effect of structure, liquid-crystalline behavior, and long-range ordering. More precisely, taking advantage of the Grignard metathesis (GRIM) polymerization[25] and of the versatility of the synthetic strategy we previously developed, a set of intricate polymeric

Scheme 1. Nomenclature and Synthetic Routes to Homopolymers $(PT_m)_n$ and $(PT_mT)_n$[a]

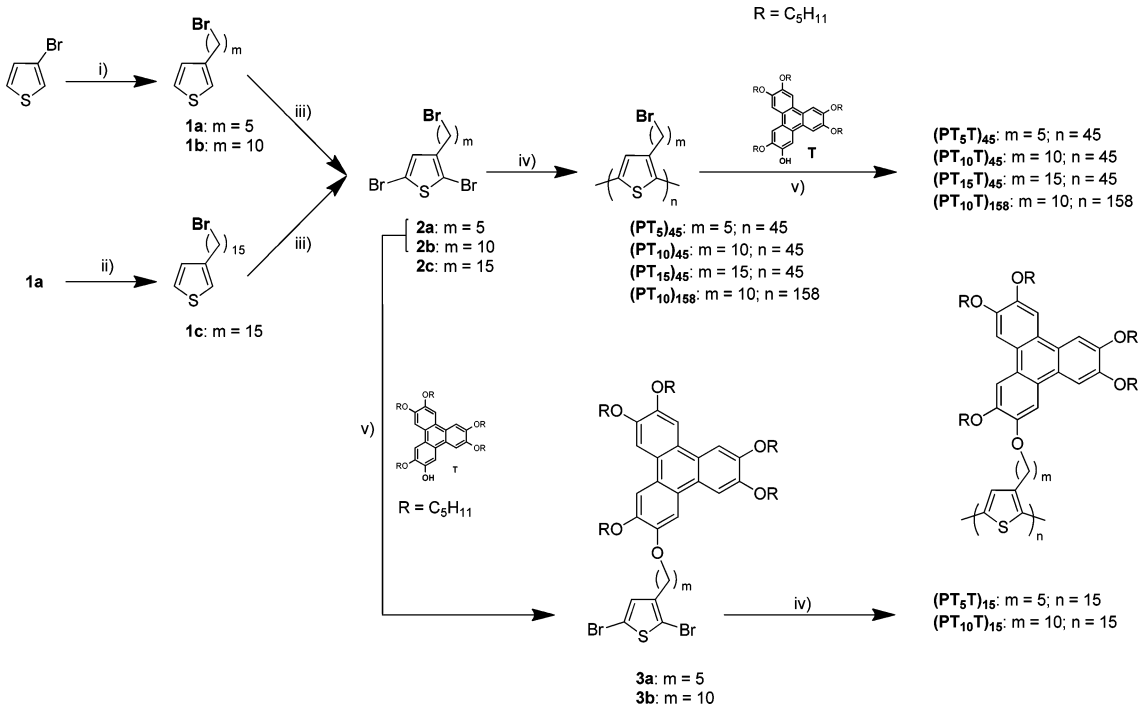

[a] m = alkyl spacer length and n = DP_n. Reagent and conditions: (i) (a) BuLi, hexane/THF, −40°C; (b) $Br(CH_2)_mBr$, −10°C/room temperature; (ii) (a) Mg, Et_2O, N_2, room temperature; (b) Li_2CuCl_4, $Br(CH_2)_{10}Br$, 0 °C, HCl; (iii) NBS, DMF, room temperature; (iv) (a) *i*PrMgCl, THF, 0 °C; (b) $Ni(dppp)Cl_2$, 0 °C/room temperature, HCl; (v) (a) K_2CO_3, DMF, **T**, 80°C; (b) $(PT_m)_n$ or **2a** and **2b**, 120 °C.

systems associating the regioregular poly(3-alkylthiophene) backbone[26] with laterally pending mesogenic triphenylenes[27] has been synthesized. Two series of polymers have been investigated, namely both homopolymers and corresponding alternating copolymers. In the former series, the pertinent structural parameters, such as (i) the length of the polymer backbones (i.e., degree of polymerization, PDI = 15, 45, 158), and (ii) the length of the aliphatic spacer between the polymeric backbone and the discotic side groups (*i.e.* $-(CH_2)_5-$, $-(CH_2)_{10}-$, $-(CH_2)_{15}-$) were systematically varied in order to evaluate impacts on the geometrical packing parameters and molecular orderings within the mesophases, eventually yielding a better understanding of the overall supramolecular organizations. The second series (alternated copolymers with thiophene/triphenylene ratios varying between 1:1 to 4:1) was synthesized in order to evaluate the influence of the controlled dilution of the mesogen, (*i.e.* the degree of polymer lateral substitution). All the new polymeric systems were fully characterized by NMR and standard polymer techniques. Their thermal and self-organization behaviors were further investigated by polarized-light optical microscopy (POM), differential scanning calorimetry (DSC) and temperature-dependent small-angle X-ray scattering (SAXS), which permitted to assess the mesophase's formation and identity, and to probe the effects of the intimate structural modifications onto the mesophase temperature ranges and symmetry. As deduced from SAXS powder measurements carried out in the temperature ranges delimited by DSC, most of the polymers self-organize into mesophases possessing intertwined lamello-columnar morphologies, though over different length-scales, resulting from the simultaneous coexistence of lamellar and columnar sublattices. The successful preparation of oriented thin films of several of these polymeric homologues allowed to use additional techniques such as atomic force microscopy (AFM), transmission electron microscopy (TEM) in bright field (BF), high-resolution (HR) and electron diffraction (ED) modes, and grazing incidence SAXS (GISAXS); these complementary techniques provided a deeper insight of the various supramolecular organizations, and permitted the complete elucidation of the structure of the lamello-columnar mesophases, resulting in an intertwined coassembly of lamellae and columns. The SCLCCP concept where the mesogen is a discotic π-conjugated molecule provides a route to elaborate polymeric materials incorporating two intercalated separate pathways toward charge carrier transport, of paramount importance for the elaboration of tomorrow's electronic, portable devices.

RESULTS

Synthesis. As just mentioned, such a comprehensive investigation requires that various sets of structurally different polymeric systems be synthesized, and whose relevant structural parameters be sequentially and independently modified. Depending on the molecular structure of the final polymer, different synthetic procedures were used, and will now be briefly described. Overall, the various homopolymers and alternating copolymers, were prepared according to the McCullough methodology, as depicted in Schemes 1 and 2, respectively (and Supporting Information). The chosen pathway for the preparation of the singly grafted homopolymers $(PT_5T)_{45}$, $(PT_{10}T)_{45}$, and $(PT_{15}T)_{45}$ was adapted from a previously described procedure.[24] It consists on the substitution of the precursory regioregular polythiophenes bearing bromide end-terminated lateral alkyl chains of various lengths, $(PT_m)_{45}$, by 1-hydroxy-penta-2,5,6,9,10-pentyloxytriphenylene derivative **T** under the standard Williamson ether reaction conditions

dx.doi.org/10.1021/ma4020356 | *Macromolecules* 2014, 47, 1715−1731

Scheme 2. Nomenclature and Synthetic Routes to Alternating Copolymers $(PBTT)_{21}$, $(PTTT)_{14}$, and $(PQTT)_9$[a]

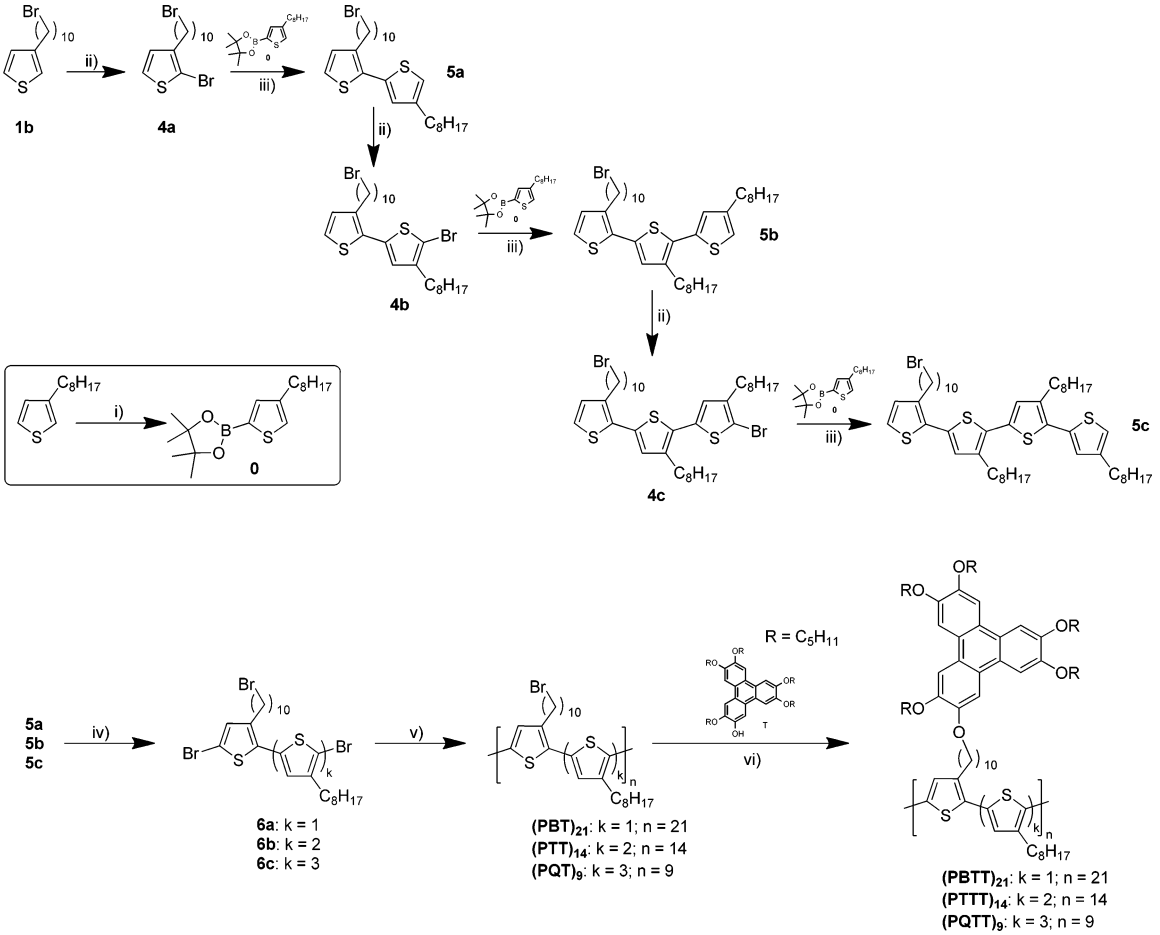

[a]Reagent and conditions: (i) LiTMP, dioxaborolane, THF, −78 °C; (ii) NBS, DMF, 35 °C; (iii) $Pd(PPh_3)_4$, 1 M $NaHCO_3$, DME, reflux; (iv) NBS, DMF, room temperature; (v) (a) iPrMgCl, THF, 0 °C; (b) $Ni(dppp)Cl_2$, 0 °C/room temperature, HCl; (vi) (a) K_2CO_3, DMF, **T**, 80 °C; (b) $(PBT)_{21}$ or $(PTT)_{14}$ or $(PQT)_9$, 120 °C.

Table 1. Characterization of Precursors and Grafted Homo-Polymers and Alternating Copolymers

polymer	M_n[a]	PDI[a]	DP_n[b]	polymer	grafting of T (%)[c]	PDI[a]	DP_n[b]
$(PT_5)_{45}$	9.8	1.2	45	$(PT_5T)_{45}$	≥95	1.2	45
$(PT_{10})_{45}$	14.7	1.2	45	$(PT_{10}T)_{45}$	≥95	1.3	45
$(PT_{15})_{45}$	19.6	1.4	45	$(PT_{15}T)_{45}$	≥95	1.5	45
$(PT_{10})_{158}$	48.2	1.2	158	$(PT_{10}T)_{158}$	≥95	3	158
–	–	–	–	$(PT_5T)_{15}$	100[e]	1.2	15
–	–	–	–	$(PT_{10}T)_{15}$	100[e]	1.3	15
$(PBT)_{21}$	10.6	1.4	42[d]	$(PBTT)_{21}$	≥95	1.6	42[d]
$(PTT)_{14}$	9.9	1.6	42[d]	$(PTTT)_{14}$	≥95	1.6	42[d]
$(PQT)_9$	8.1	1.6	36[d]	$(PQTT)_9$	≥95	1.6	36[d]

[a]M_n = Number-average molecular weight (kDa) and PDI = Polydispersity index, determined by gel permeation chromatography (GPC) in THF relative to polystyrene standards. [b]Determined by ^1H NMR. [c]The conversion is quasi-complete at the accuracy of the NMR, as shown by the total vanishing of the proton of the ^1H NMR resonance of the methylene group (δ = 3.40 ppm) in the α position to the terminal bromine atom. [d]Considering every thiophene monomers as equivalent. [e]**T** was already grafted on monomers.

(Scheme 1). The substitution of the $(PT_m)_{45}$ backbones by the discotic triphenylenes was evidenced by the vanishing of the ^1H NMR resonance of the methylene group (δ = 3.40 ppm) in the α position to the terminal bromine atom,[25c,28] the molecular weight increase from size exclusion chromatography (Figures S1 and S2 in Supporting Information) and the composition change from elemental analysis (Supporting Information), respectively. However, the substitution reaction is unlikely to be quantitative in account of the pending group size, and considering the sensitivity of the NMR method, the yield can be estimated to lie between 95% and 100%. The precursory polythiophenes $(PT_5)_{45}$, $(PT_{10})_{45}$, and $(PT_{15})_{45}$ were prepared according to the Grignard metathesis (GRIM),[25] which led to well-defined polymeric architectures with narrow polydispersity indices (PDI ranging between 1.2 and 1.4) and highly controlled molecular-weights (degree of polymerization, DP_n = 45), as determined by gel permeation chromatography (GPC) and NMR spectroscopy, respectively (Table 1). By

dx.doi.org/10.1021/ma4020356 | Macromolecules 2014, 47, 1715−1731

reducing the molar ratio of the monomer to the nickel catalyst (acting as initiator) in GRIM method, one longer precursory analogous polymer $(\mathbf{PT}_{10})_{158}$ (i.e., with DP_n = 158, PDI = 1.2) was also prepared similarly, and then substituted by the triphenylene derivative **T**, leading to the longer-grafted homopolymer $(\mathbf{PT}_{10}\mathbf{T})_{158}$.

This series of polymers was completed by two more shorter grafted homologues with a pentyl and decyl spacer, $(\mathbf{PT}_5\mathbf{T})_{15}$ and $(\mathbf{PT}_{10}\mathbf{T})_{15}$, respectively, also prepared by Grignard metathesis, but starting from the 2,5-dibromothiophene monomeric derivatives, **3a** and **3b**, that are already bearing the triphenylene side-group **T** (Scheme 1). This procedure also led to well-defined polymeric architectures, with an average DP_n value (15 thiophene units) and low PDI (ca. 1.2−1.4). The detailed protocols for the preparation of all the starting building blocks **1a−c**, monomers **2a−c**, **3a−b**, and polymers are given in Supporting Information.

To complete this systematic study, we also undertook the synthesis of three alternating grafted copolymers, namely $(\mathbf{PBTT})_{21}$, $(\mathbf{PTTT})_{14}$ and $(\mathbf{PQTT})_9$ (Scheme 2). In this case, the precursory regioregular alternating copolythiophenes, $(\mathbf{PBT})_{21}$, $(\mathbf{PTT})_{14}$, and $(\mathbf{PQT})_9$, possess one bromide end-terminated lateral decyl chain, regularly alternating with one, two or three 3-octylthiophene units, respectively. They were obtained with controlled polymeric architectures (DP_n = 36−45 and PDI = 1.4−1.6) (Table 1) by GRIM polymerization of the dibromo bis-, ter- or quaterthiophene monomers **6a−6c**, respectively (Scheme 2).[29] The intermediate bi-, ter- or quaterthiophene key-synthons **5a−5c** were prepared following an iterative palladium(0)-catalyzed Suzuki coupling procedure between 2-bromo-3-(10-bromodecyl)-thiophene **4a**, obtained by bromination of octylthiophene, **1b**, with the boronic ester derivative of 3-octylthiophene, **0**, leading to the head-to-tail coupling compound **5a**; this process, bromination-Suzuki coupling, was repeated twice (**5a** → **4b**, **4b** → **5b**; **5b** → **4c**, **4c** → **5c**); these three oligothiophene, **5a−5c**, were then converted into their dibromo derivatives, **6a−6c**. The final regioregular copolythiophenes, $(\mathbf{PBTT})_{21}$, $(\mathbf{PTTT})_{14}$, and $(\mathbf{PQTT})_9$, were obtained by the grafting of the triphenylene derivative onto the corresponding polythiophene backbones, $(\mathbf{PBT})_{21}$, $(\mathbf{PTT})_{14}$, and $(\mathbf{PQT})_9$, respectively using etherification reaction. The synthetic details of all building blocks **0**, **4a−4c**, **5a−5c**, and **6a−6c** and alternating copolythiophenes are given in Supporting Information. It is worth noticing that the final copolythiophenes, $(\mathbf{PBTT})_{21}$, $(\mathbf{PTTT})_{14}$, and $(\mathbf{PQTT})_9$, show somewhat higher PDIs than their homologous homopolymers. This higher polydispersity could be explained by the influence on the insertion of unusually long monomers, containing several thiophene units onto the chain-growth process. The low polymerization degrees are further indicators of the modified conditions of the polymerization reaction.

Thermal and Mesomorphic Behavior (POM and DSC). Preliminary investigations of the thermal behavior of all the polymers were performed by POM and DSC techniques, prior to SAXS measurements. Almost none of the polymers under study exhibit specific LC textures with identifiable characteristic patterns or defects. Birefringence combined to liquid-like behavior was nevertheless observed by POM, for most of the polymers, revealing the existence of liquid-crystalline mesophases. On cooling from the isotropic state, birefringent textures are recovered and maintained down to room temperature without crossing another phase transition. The homopolymers of the $(\mathbf{PT}_{10}\mathbf{T})_n$ subseries (n = 15, 45 and 158, including the polymer previously reported, n = 45)[24] produce viscous textures (Figure S3a,b, Supporting Information), even on very slow cooling from the isotropic liquid phase, inhibiting the development of the mesophase natural textures. At high temperature, $(\mathbf{PT}_{15}\mathbf{T})_{45}$ gives rise to somewhat more fluid POM textures with coexistence of birefringent and homeotropic regions, characteristic of a uniaxial mesophase (Figure S3c). The two homopolymers with pentyl spacers ($(\mathbf{PT}_5\mathbf{T})_{45}$ and $(\mathbf{PT}_5\mathbf{T})_{15}$) reveal highly fluid POM textures at high temperature, with structural defects typical of the nematic phase (Figure S3d,e). Finally, the same observations as above for $(\mathbf{PT}_{10}\mathbf{T})_n$ polymers apply for the alternated copolymer $(\mathbf{PBTT})_{21}$ with one octylthiophene per repeat monomeric unit (Figure S3f); in contrast, copolymers with higher amounts of octylthiophene ($(\mathbf{PTTT})_{14}$ and $(\mathbf{PQTT})_9$) appear amorphous at all temperatures (no texture), and do not seem to exhibit mesomorphism. All these results are consistent with DSC and SAXS measurements (vide infra).

DSC traces obtained for this series of polymers are quite typical of high-molecular weight compounds, and contain signals characteristic of glass transitions, and, at higher temperature, broad exothermic transitions corresponding to the clearing into the isotropic liquid, the latter in agreement with those detected by POM. Homopolymers of the $(\mathbf{PT}_{10}\mathbf{T})_n$ subseries show a first heating run different from those recorded on subsequent heating/cooling cycles. For instance, the first heating of $(\mathbf{PT}_{10}\mathbf{T})_{158}$ contains an additional annealing exothermic peak besides the glass transition and the isotropization (Figure S4a), coinciding with an irreversible structural transformation, as later evidenced by SAXS. The first heating of $(\mathbf{PT}_{10}\mathbf{T})_{15}$ contains a broad signal in the temperature range of the annealing reorganization (also evidenced by SAXS, Figure S5a), but unlike $(\mathbf{PT}_{10}\mathbf{T})_{158}$, the formation process of the mesophase takes several hours upon cooling. The homopolymer with the pentadecyl spacer ($(\mathbf{PT}_{15}\mathbf{T})_{45}$) shows reproducible traces on both heating and cooling, with a substantial delay of the clearing temperature on cooling from the disordered state, thus reducing the mesophase temperature range accordingly (Figure S5c). Finally, the two homopolymers with the short spacer ($(\mathbf{PT}_5\mathbf{T})_{15}$ and $(\mathbf{PT}_5\mathbf{T})_{45}$) exhibit undefined, irreversible signals during the first heating and heat flow drifts over an extended temperature range, which are not associated with significant changes in the SAXS patterns (vide infra), and more likely related to the fluidification of the sample and/or to an annealing process (Figures S4b, S5b).

The alternated copolymer $(\mathbf{PBTT})_{21}$ shows a thermal behavior similar to $(\mathbf{PT}_{10}\mathbf{T})_{15}$, with the occurrence of a broad signal in the temperature range of the annealing reorganization during the first heating, and signals characteristic of both a glass transition and the isotropization, on subsequent heating/cooling cycles (Figure S6a). In contrast, the absence of any mesomorphic behavior is confirmed for both copolymers with high octylthiophene contents ($(\mathbf{PTTT})_{14}$ and $(\mathbf{PQTT})_9$). DSC traces of $(\mathbf{PTTT})_{14}$ only show the signal corresponding to the glass transition, near 10 °C, with a very good reproducibility (Figure S6b). $(\mathbf{PQTT})_9$ however shows an additional broad endotherm between 40 and 80 °C during the first heating run but solely a glass transition in subsequent heat−cool cycles, in accordance with amorphous behavior. A small endotherm reappears on heating after several day aging at room temperature (Figure S6c).

Characterization of the Mesophases Structures by SAXS. The X-ray patterns of the homopolymers $(\mathbf{PT}_{10}\mathbf{T})_n$

dx.doi.org/10.1021/ma4020356 | Macromolecules 2014, 47, 1715−1731

recorded as a function of temperature (Figure 1) contain several sharp Bragg reflections in the small-angle region and

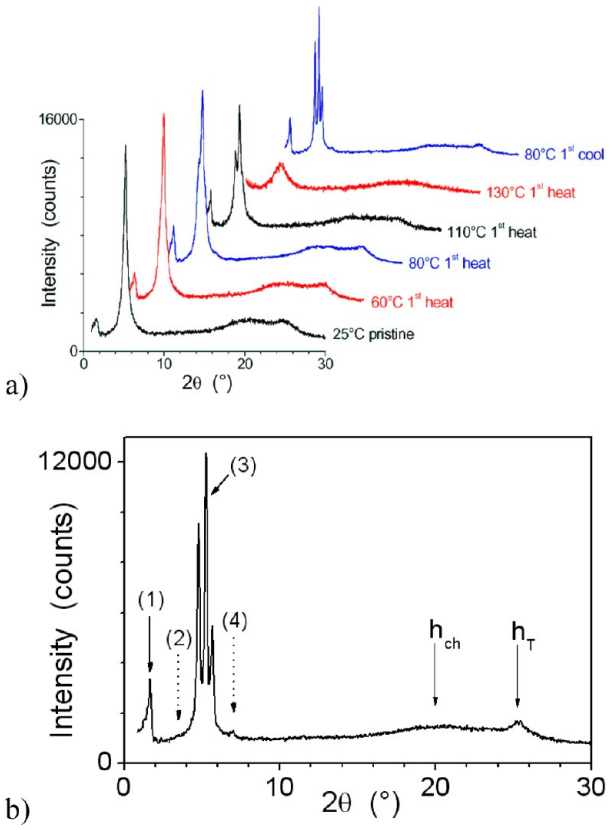

Figure 1. (a) SAXS patterns of $(\mathbf{PT_{10}T})_{158}$ recorded during the first heat−cool cycle and (b) SAXS pattern of the same polymer after the first cycle at 50 °C [(n), nth lamellar order reflection; h_{ch} and h_T, scattering signals from lateral distances between molten aliphatic chains and from the triphenylene π−π stacking distance].

two scattering halos in the wide-angle region. The broader scattering corresponds to the molten state of the aliphatic chains, h_{ch}, and reflects the liquid nature of the mesophase, while the second signal at larger angle is associated with the triphenylene cores π−π stacking distance, h_T, and thus to the presence of columns. As for the analogous $(\mathbf{PT_{10}T})_{45}$ previously reported (Figure S7), the set of sharp and intense small-angle reflections (Figures 1b, S8) in the final "annealed" state comes from a lamello-columnar structure (vide infra, Tables 2 and 3). The sharpness of the small-angle reflections indicates that both lamellae and 2D lattice of columns are long-range correlated, but note that the lamellar orders become sharp faster than the reflections of columnar registry during the annealing process. The small-angle region indeed only contains two broad peaks in the pristine state; their location coincides with the main reflections of the annealed pattern, which is indicative of a mesophase preorganization in small domains (referred thereafter as Cyb for cybotaxis, Figure 1a).

The analogue homopolymer with pentadecyl spacers ($(\mathbf{PT_{15}T})_{45}$) shows cybotactic (pristine state) and liquid-crystalline organizations (annealed state) similar to the above set of homopolymers, except for a thicker lamellae (the periodicity d increases from 5.0 to 5.8 nm) and a depleted columnar character. Indeed, besides the numerous sharp lamellar orders (Figure 2, numbered 1−5, Table 3), the small-angle region only contains a weak scattering from the short-range correlated arrangement of columns (Figure 2, inset). In the wide-angle region two broad scattering maxima h_T and h_{2T} reveal the loose piling of triphenylene rings into columns and a dimer modulation within piles (Figure 2).

Ordering in the last two related homopolymers with the shorter spacer, ($(\mathbf{PT_5T})_{45}$ and $(\mathbf{PT_5T})_{15}$), is considerably reduced with respect to those discussed above, as evidenced by the X-ray patterns now showing only small-angle diffuse signals (periodicities of ca. 3.7 nm, Figures 3 and S9). This is in consistency with a nematic type of organization (POM), but the presence of 3 additional broad harmonics (in the ratio 1:2:3:4, Table 4) is very unconventional for a local-range periodicity, as well as the wide-angle signal (Figures 3 and S9, h_T), both features that are indicative of the persistence of the lamello-columnar organization at the local nematic scale. These patterns are discussed below, in connection to the effect of the spacer-length (vide infra).

As inferred from POM and DSC, only one copolymer appears to be mesomorphous. The lamello-columnar mesophase of $(\mathbf{PBTT})_{21}$ gives rise to similar SAXS patterns and shows a similar lattice geometry ($d \approx 5.2$ nm) as the related homopolymer, except the presence of more lamellar orders and less reflections specific of the columnar lattice (Figure 4a, Table 3). This reinforced lamellar character is concomitant with the

Table 2. Mesophase Organizations and Transition Temperatures of the Homopolymers and Alternating Copolymers

polymer[a]	pristine state[b]	annealed state[c]	T_G [°C][d]	T_{ann} [°C][e]	T_{iso} [°C][f]
$(\mathbf{PT_{10}T})_{158}$	Cyb_{LamCol}	$LamCol_R$	15	70−80	114−122
$(\mathbf{PT_{10}T})_{45}$	Cyb_{LamCol}	$LamCol_R$	15	50−60	101−107
$(\mathbf{PT_{10}T})_{15}$	Cyb_{LamCol}	$LamCol_R$	7	20−50	96−98
$(\mathbf{PT_{15}T})_{45}$	Cyb_{LamCol}	Lam_{Col}	−2	50−60	62−82
$(\mathbf{PT_5T})_{45}$	–	N_{LamCol}	35	40−140	160−170
$(\mathbf{PT_5T})_{15}$	–	N_{LamCol}	30	40−140	155−162
$(\mathbf{PBTT})_{21}$	Cyb_{LamCol}	$LamCol_R$	13	70−110	123−134
$(\mathbf{PTTT})_{14}$	Iso	–	11	–	–
$(\mathbf{PQTT})_9$	Iso	–	1	–	–

[a]Polymer nomenclature. [b]Cyb_{LamCol}: lamello-columnar short-range correlated preorganization. Iso: isotropic phase, i.e., amorphous state without lamellar and columnar preorganizations. [c]Mesophase obtained during the first heating above the annealing temperature and on cooling from the isotropic phase. $LamCol_R$: lamello-columnar phase with rectangular sublattice. Lam_{Col}: lamellar phase with short-range correlated columnar registry. N_{LamCol}: nematic phase with lamello-columnar local order. [d]Glass transition temperature (step midpoint from 2nd heating DSC curves). [e]Annealing temperature range (transformation from the pristine state in the mesophase organization on first heating), estimated from SAXS and DSC. [f]Isotropization temperature range estimated from onset and maximum in 2nd heating DSC curves.

dx.doi.org/10.1021/ma4020356 | Macromolecules 2014, 47, 1715−1731

Table 3. Reflections Indexation of the SAXS Patterns Recorded at the Temperature T, in the Lamello-Columnar Phase with Rectangular *p2gg*[34] Lattice ($LamCol_R$) for $(PT_{10}T)_{158}$, $(PT_{10}T)_{45}$, $(PT_{10}T)_{15}$, and $(PBTT)_{21}$ and in the Lamellar Phase with Medium-Range Ordered Columnar Registry (Lam_{Col}) for $(PT_{15}T)_{45}$

			$(PT_{10}T)_{158}$		$(PT_{10}T)_{45}$		$(PT_{10}T)_{15}$		$(PBTT)_{21}$		$(PT_{15}T)_{45}$	
		Rect.	$LamCol_R$		$LamCol_R$		$LamCol_R$		$LamCol_R$		Lam_{Col}	
	Lam[a]	*p2gg*[b]	T = 50 °C		T = 50 °C		T = 80 °C		T = 80 °C		T = 50 °C	
no.	l	h k	d [Å][c]	I[d]	d [Å][c]	I[d]	d [Å][c]	I[d]	d [Å][c]	I[d]	d [Å][c]	I[d]
1	1	2 0	50.9	VS	50.2	VS	50.8	VS	51.9	VS	58.6	M
2	2	4 0	25.4	W	25.6	W	25.4	W	25.9	VW	29.3	W
3		2 2	18.58	VS	18.3	VS	18.70	VS	18.49	S		
4	3	6 0	16.82	VS	16.6	VS	16.86	VS	17.26	VS	19.48	S
5		4 2	15.70	VS	15.5	VS	15.76	VS	15.75	S		
6	4	8 0	12.72	W	12.7	W	12.70	W	12.97	W	–	–
7		8 2	10.66	VW	10.5	VW	10.71	VW	–	–		
8	5	10 0	–	–	–	–	10.16	VW	10.38	W	11.72	W
9		2 4	9.79	VW	9.9	W	9.77	VW	–	–		
10	6	12 0	–	–	–		–	–	8.65	W	9.77	W
11		8 4	–	–	7.7	VW	7.88	VW	–	–		
12	7	14 0	–	–	–	–	–	–	7.41	W	10.5	VW
13		10 4	–	–	7.1	VW	–	–	–	–		
14	8	16 0	–	–	–	–	–	–	6.49	VW	–	–
	d_T (ξ, I) [Å]		–		–		–		–		18.0 (150, S)	
	h_{2T} (ξ, I) [Å]		–		–		–		–		7.3 (30, M)	
	h_{ch} (ξ, I) [Å]		4.3 (10, VS)		4.4 (10, VS)		4.3 (10, VS)		4.4 (10, VS)		4.4 (10, VS)	
	h_{PT} (ξ, I) [Å]		–		–		–		3.81 (85, M)		–	
	h_T (ξ, I) [Å]		3.56 (60, M)		3.56 (70, M)		3.55 (60, W)		3.56 (40, M)		3.53 (20, W)	
			d = 50.53 Å		d = 50.18 Å		d = 50.77 Å		d = 51.88 Å		d = 58.62 Å	
			N_{Trow} = 3		N_{Trow} = 3		N_{Trow} = 3		N_{Trow} = 3		N_{Trow} = 3	
			a = 2d = 101.1 Å		a = 2d = 100.4 Å		a = 2d = 101.5 Å		a = 2d = 103.8 Å			
			b = 2a_T = 39.9 Å		b = 2a_T = 39.6 Å		b = 2a_T = 40.0 Å		b = 2a_T = 39.6 Å		2a_T ≈ 37.8 Å	
			S = 4036 Å^2		S = 3972 Å^2		S = 4066 Å^2		S = 4105 Å^2		(ξ/a$_T$ ≈ 8)	
			$N_{PT} \approx N_T$ = 12		$N_{PT} \approx N_T$ = 12		$N_{PT} \approx N_T$ = 12		N_{PT} ≈ 24; N_T = 12			
			S_{T+PT} = 336 Å^2		S_{T+PT} = 331 Å^2		S_{T+PT} = 339 Å^2		S_{T+PT} = 342 Å^2		S_{T+PT} ≈ 369 Å^2	
			V_M ≈ 1378 Å^3		V_M ≈ 1378 Å^3		V_M ≈ 1408 Å^3		V_M ≈ 1712 Å^3		V_M ≈ 1516 Å^3	
			A = 2A_T ≈ 327 Å^2		A = 2A_T ≈ 330 Å^2		A = 2A_T ≈ 333 Å^2		A = 2A_T ≈ 396 Å^2		2A_T ≈ 310 Å^2	
			h ≈ 8.19 Å		h ≈ 8.33 Å		h ≈ 8.31 Å		h ≈ 10.01 Å		h ≈ 8.21 Å	

[a]Indexation of the lamellar orders. [b]Indexation of the reflections of the lamello-columnar lattice. [c]Measured spacing. [d]Intensity (VS, very strong; S, strong; M, medium; W,: weak; VW, very weak; –, missing); ξ, for diffuse reflections, correlation length from Scherrer formula; d_T, diffuse reflection from columnar registry; h_{2T}, triphenylene dimers stacking distance; h_{ch}, lateral distances between molten aliphatic chains; h_{PT}, polythiophene backbone π–π-stacking distance; h_T, triphenylene π–π-stacking distance; d, N_{Trow}, layer spacing and number of triphenylene column rows per lamella; a, b, S, N_{PT}, N_T, parameters of the columnar lattice, lattice area, number of backbones, and number of columns in the bidimensional lattice; a_T, spacing within rows (in the Lam_{Col} phase, d_T is assimilated to the reflection (11) of the average lattice $a_T \times d$); $S_{T+PT} = d \times a_T/N_{Trow}$, cross-section area per column including spacer and backbone; V_M, volume of the repetition unit; A, $A_T = 2N_{Trow} \times V_M/d$, "packing area" and section of a single column in the plane of the lamellae; $h = 2V_M/S_{T+PT}$, periodicity in perpendicular to the lattice plane.

appearance in the wide-angle region of an additional scattering due to the stacking of polythiophenes (h_{PT}) (the attribution is confirmed with reference patterns, see Figure S10 in Supporting Information). The vanishing of the mesophase for **(PTTT)$_{14}$** results in X-ray patterns with only small-angle scattering due to intermolecular distances, characteristic of the amorphous state (Figure 4b). The same pattern is observed for **(PQTT)$_9$** above 100 °C, but below this temperature the small-angle scattering signal shape gradually evolves toward two reflections in the spacing ratio 1:2 while the h_{PT} maximum grows on the wide-angle scattering. With correlation lengths in the 200 Å range on cooling, the systems turns out to be very close to a mesophase based on segregated polythiophene lamellae (Figure S11). Strictly speaking, structures at high and low temperatures are just different states of the same amorphous phase, since neither a POM texture nor a DSC peak could be observed. Though, this embryonic segregation at low-mesogen content likely prefigures the lamellar structure of the neat semicrystalline polyalkylthiophene.

The mesomorphic characteristics of the polymers and polymorphic data are listed in Table 2. Positions and widths of all reflections, precisely measured on the SAXS patterns, and correctly indexed, are gathered in Tables 3 and 4, and commented in combination with additional information from oriented thin films.

Summarizing, SAXS powder measurements (along POM and DSC) partly reveal the intricate nature of the various mesophases formed by these sets of triphenylene-functionalized polymers. Three regimes could be distinctively observed: (i) polymers deprived of mesomorphism, i.e., the copolymers with high thiophene/triphenylene ratios, (ii) polymers displaying a low-ordering nematic mesophase, i.e., those with a short lateral spacer between the backbone and the triphenylene, and (iii) polymers with decyl or longer spacers showing highly ordered

dx.doi.org/10.1021/ma4020356 | Macromolecules 2014, 47, 1715–1731

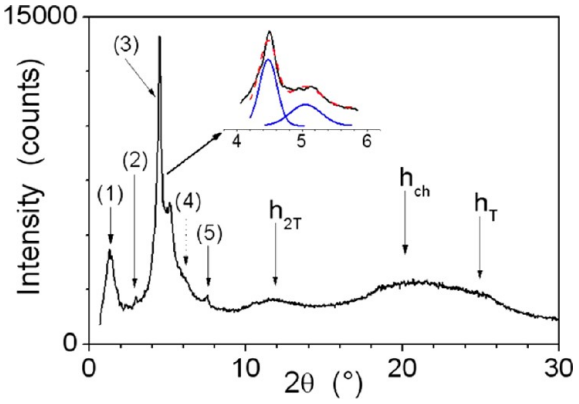

Figure 2. SAXS pattern of $(PT_{15}T)_{45}$ at 50 °C on cooling from isotropic state. Inset view: pattern with improved resolution at low angle and diffraction peak superposition [Labels defined as in Figure 1].

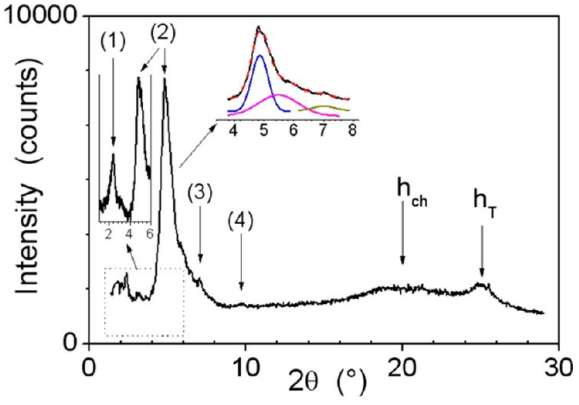

Figure 3. SAXS pattern at 80 °C on cooling of polymer $(PT_5T)_{45}$. Inset view: pattern with improved resolution at low angle and diffraction peak superposition [labels defined as in Figure 1].

mesophases, provisionally identified as lamello-columnar, all having a long-range lamellar sublattice, resulting likely from polythiophene segments arranged into parallel rows, interplayed with a 2D sublattice, generated by the one-dimensional stacking of the triphenylene cores and the subsequent columnar layout. The absence of aligned samples and the nonobservation of additional cross-reflections (*hkl*) however did not permit to retrieve the respective orientations and connections between both sublattices, and thus to ultimately elucidate the mesophase structure. We thus attempted other techniques of alignment specific of conjugated polymers, actually conceivable because of the presence of the polythiophene moiety. Nanometer scale thin films prepared by the drop flow casting method showed regions with some orientations when analyzed by AFM. Going on polymer thin film techniques, we then resorted to use directional epitaxial crystallization (DEC), in order to prepare samples suitable for TEM-ED and GISAXS. The complementary information accessed in that way provided a deeper insight in the various supramolecular organizations, and permitted the complete elucidation of the structure of the lamello-columnar mesophases, as reported now.

Atomic Force Microscopy Study of Oriented Polymeric Thin Films. The morphology of the $(PT_{10}T)_{45}$ and $(PT_5T)_{45}$ thin films on surfaces was first studied using tapping mode atomic force microscopy (AFM). A $(PT_{10}T)_{45}$ thin film was successfully prepared from an octane hot solution (75 μg/mL) by flow casting process on an OTS treated silicon substrate,[30] then annealed at 90 °C for 20 min. The AFM topography and phase images show a nanostructured film with terraces (Figure 5a,b), indicative of extended flat lamellae oriented parallel to the substrate surface. The heights of the terraces determined from topography images were about 10 nm, 5 nm or multiples of 5 nm (Figures 5c,d and S12). They coincide well with the lamellar periodicity of the bulk structure measured from SAXS patterns (Table 3). A $(PT_5T)_{45}$ thin film was also prepared, but from a concentrated $CHCl_3$ solution (2.5 mg/mL) by similar flow casting process on a cleaned bare silicon substrate (without OTS), then annealed at 130 °C for 20 min. The AFM phase images reveal a good molecular resolution. They display a nanostructured film with a number of thin stripes, periodically stacked within lamellae-type structures, as underlined on the left of Figure 5e. The spacing between the lamellae (e.g., between consecutive dark stripes) ranges between ten and several tens of nanometers and is thus a priori compatible with the average backbone length of 17 nm (DP_n = 45; DPI = 1.2), confirming that the regions between two consecutive lamellae are constituted by the polymers ends, which may correspond to amorphous zones (Figure 8f).[31] Between these zones, the organized domains result from the lateral self-assembly of the main polymers segments predominantly face-on on the substrate surface. An additional substructure is moreover observed in the bright domains in the direction perpendicular to the backbones (Figure 5f),

Table 4. SAXS Patterns at the Temperature *T*, in the Nematic Phase with Lamello-Columnar Local Organization (N_{LamCol}) for $(PT_5T)_{45}$ and $(PT_5T)_{15}$

	$(PT_5T)_{45}$			$(PT_5T)_{15}$		
Cyb.	N_{LamCol}			N_{LamCol}		
Lam	T = 80 °C			T = 80 °C		
l^a	d [Å]^b	ξ [Å]^c	I^d	d [Å]^b	ξ [Å]^c	I^d
1	37	160	M	37.5	120	M
2	18.2	120	VS	18.3	100	VS
3	12.6	100	M	12.5	100	M
4	9.2	100	VW	9.2	100	VW
D_T	16.1	50	VS	15.9	40	VS
h_{ch}	4.4	10	VS	4.4	10	VS
h_T	3.54	40	S	3.54	4	S
	d = 36.9(2) Å			d = 36.9(4) Å		
	$(\xi_\parallel/d \approx 3)$			$(\xi_\parallel/d \approx 3)$		
	N_{Trow} = 2			N_{Trow} = 2		
	$D_\perp = D_T \approx 16.1$ Å			$D_\perp = D_T \approx 15.9$ Å		
	$(\xi_\perp/D_\perp \approx 3)$			$(\xi_\perp/D_\perp \approx 2.5)$		
	$S_{T+PT} \approx 297$ Å^2			$S_{T+PT} \approx 294$ Å^2		
	$V_M \approx 1267$ Å^3			$V_M \approx 1267$ Å^3		
	$2A \approx 275$ Å^2			$2A \approx 274$ Å^2		
	$h \approx 8.53$ Å			$h \approx 8.63$ Å		

[a]Indexation of reflections from local-range ordered lamellae (cyb lam. for cybotactic lamellae) of column dimers. [b]Measured spacing. [c]Correlation length from Scherrer formula. [d]Intensity. D_T: lateral distances between dimers. h_{ch}: lateral distances between molten aliphatic chains. h_T: triphenylene $\pi-\pi$-stacking distance (Table 3). *d*, N_{Trow}: thickness of cyb. lamellae and number of rows of half dimers per lamella. $D_\perp$: distance between dimers within rows. $S_{T+PT} = d \times D_T/N_{Trow}$: area per half dimer in the plane of dimer stacks. V_M: volume of the repetition unit. $A_\perp = 2N_{Trow} \times V_M/d$: area per dimer in the plane of the cyb. lamellae. $h = 2V_M/S_{T+PT}$: periodicity along the stacking direction of dimers.

dx.doi.org/10.1021/ma4020356 | *Macromolecules* 2014, 47, 1715−1731

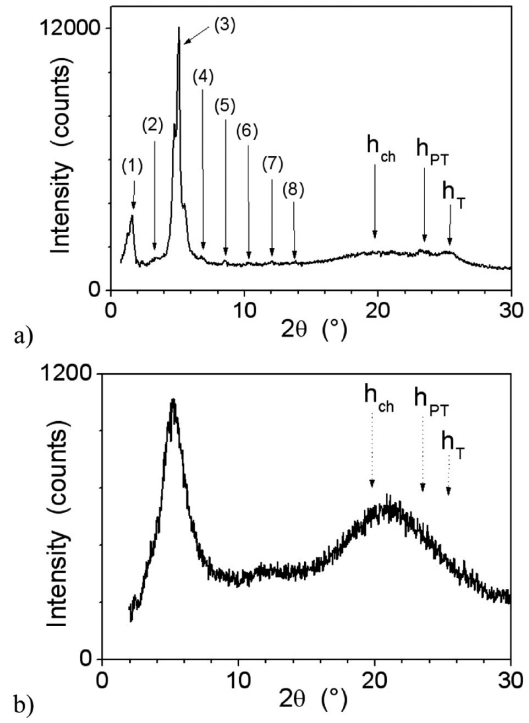

Figure 4. SAXS patterns of (a) $(\mathbf{PBTT})_{21}$ at 50 °C on cooling from isotropic state, and (b) of $(\mathbf{PTTT})_{14}$ at 50 °C in the amorphous state [labels defined as in Figure 1; h_{PT}, scattering signal from the polythiophene backbone $\pi-\pi$ stacking distance, Figure S10].

whose periodicity of about 3.8 nm coincides with the periodicity of the short-range correlated layering, evidenced in SAXS patterns (Table 4). This coincidence means that the layers embryos formed by the alternation of backbones and side groups mainly lie in the plane of the substrate, presumably due to the epitaxial orientation of the polythiophene chains on the bare silicon substrate.

TEM and GISAXS Studies of Oriented Thin Films of $(\mathbf{PT}_m\mathbf{T})_n$ by DEC. Nanostructured oriented films of a few tens of nanometers thickness with several polymers were fabricated by using the directional epitaxial crystallization method with 1,3,5-trichlorobenzene (TCB, conditions described in Supporting Information). The films of the longest polymer ($(\mathbf{PT}_{10}\mathbf{T})_{158}$) all contain large regions with uniform in-plane alignment, making possible a detailed investigation by TEM, ED and GISAXS. In contrast, the same preparation conditions used for $(\mathbf{PT}_{10}\mathbf{T})_{15}$ led to thin films exclusively constituted by amorphous or nonoriented zones, which do not provide access to any further structural information. Films of $(\mathbf{PT}_{15}\mathbf{T})_{45}$ and $(\mathbf{PT}_5\mathbf{T})_{45}$ were also obtained as poorly structured and oriented, but small zones suitable for ED analysis could nevertheless be selected. These observations are consistent with bulk properties and AFM results. For $(\mathbf{PT}_{10}\mathbf{T})_{15}$ and $(\mathbf{PT}_{15}\mathbf{T})_{45}$, the mesophase domains in POM textures grow slowly from the isotropic melt and the isotropic phase is maintained below the melting temperature of TCB (63 °C) or even down to room temperature in DSC cooling runs. In contrast, the transition from the isotropic state of $(\mathbf{PT}_{10}\mathbf{T})_{158}$ is weakly delayed and becomes complete above the temperature of directional solidification. The differences in the thin films quality might therefore be the consequence of the variation of the isotropization temperature in the polymer series. It is tempting to attribute this variation to the influence of the backbone length onto the constitution of well-structured large-size polymer lamellae, but previous study on P3HT films evidenced an improved crystallinity for the shortest polymers (although the polymerization degrees were slightly higher, ranging from 34 to 206).[32] More likely, the stabilization of the mesophase organization for the long backbone is due to an improved microsegregation of the pending mesogens, but the involved mechanism is not clear yet.

The availability of thin films of $(\mathbf{PT}_{10}\mathbf{T})_{158}$ permits one to perform further and more detailed structural investigations. Optical microscopy of $(\mathbf{PT}_{10}\mathbf{T})_{158}$ films evidenced a maximum of absorption coinciding with the growing direction of TCB crystals (c_{TCB}) associated with a high birefringence between crossed polarizers, which is a sign for the alignment of the polymer backbones parallel to c_{TCB}. This is confirmed by TEM BF images (Figure 6a) showing a uniformly oriented alternation of dark and bright stripes. The contrast in the TEM BF image is obtained by the use of a small objective aperture that cuts off the diffracted electrons i.e. dark stripes correspond to crystalline lamellae and bright regions to interlamellar amorphous zones. As inferred from the Fourier transform of the BF image (inset, Figure 6a), a characteristic 30-nm lamellar periodicity, almost identical to that observed for P3HT films oriented on TCB, is observed.[13b] This observation suggests that the characteristic lamellar structure is enforced by the epitaxial orientation of the polythiophene backbone, regardless of the presence of lateral pending triphenylene moieties. This result further indicates that $(\mathbf{PT}_{10}\mathbf{T})_{158}$ is semicrystalline with the coexistence of disordered zones that alternate with domains of crystalline "P3HT" segments. This implies that the polythiophene backbone can fold despite the presence of bulky pending triphenylenes. Folding is further supported by the fact that the contour length of the chain ($L \approx 60$ nm for DPn ≈ 158) exceeds clearly the lamellar period observed by TEM. In other words, the amorphous interlamellar zones may contain folds, tied-chains, and chain-ends.

Using low-dose HR-TEM, the crystalline lamellae display a substructure, i.e. a periodic fringed pattern (Figure 6b), with a 5-nm periodicity in the direction perpendicular to the polymer backbone. In P3HT, a similar fringed pattern is observed within crystalline lamellae but with a 1.65 nm period corresponding to the distance between two layers of π-stacked polythiophene backbones separated by one layer of alkyl side-chains. The contrast in the HR-TEM image is due to the alternation of π-stacked polythiophene backbones containing sulfur atoms and the layers of alkyl side-chains containing only the lighter C and H atoms. This contrast can only be observed if the π-stacking direction of the **PT** chains coincides with the direction of incident electron beam. In the present case, we can propose a similar origin for the contrast in the HR-TEM image, but the π-stacked polythiophene chains are separated by a much larger distance due to the presence of the bulky triphenylenes whereby increasing the interchain distance to 5 nm. Regarding the stem length in the crystalline lamellae, it amounts to 10−12 nm, to be compared to the 30 nm total lamellar period (crystalline+amorphous). This value is similar to that observed for high-molecular weight P3HT.[33]

The observation of a fringed pattern in HR-TEM with a 5-nm period is fully consistent with the SAXS results evidencing a lamellar sublattice with the same characteristic period of 5 nm. ED patterns (Figure 7) confirm this attribution and show that the intensity within the lamellar reflection series is maximum for the third order, evidencing that the (003) reflection of the

dx.doi.org/10.1021/ma4020356 | Macromolecules 2014, 47, 1715−1731

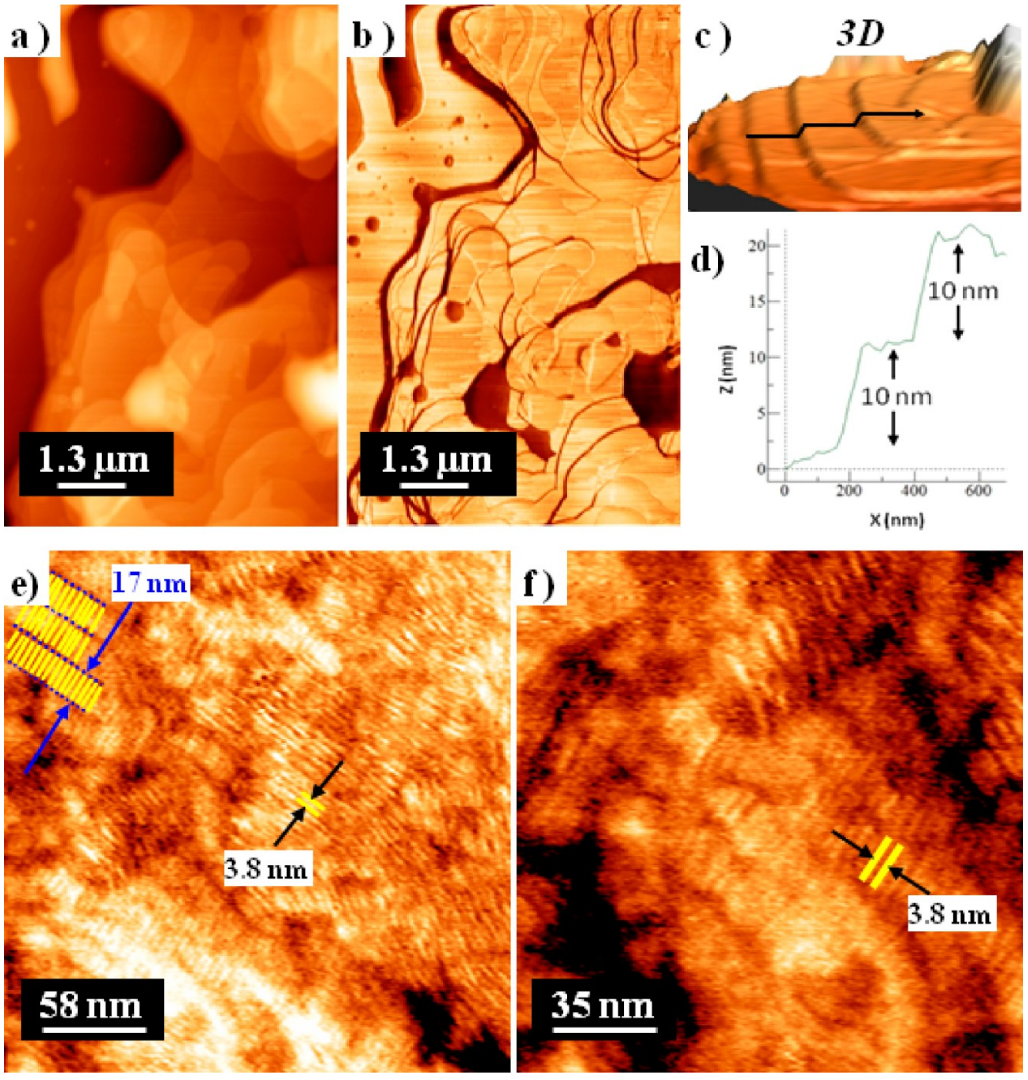

Figure 5. (a) Topography and (b) phase AFM images of $(PT_{10}T)_{45}$ thin film on silicon wafer treated with the silylating agent octadecyltrichlorosilane (OTS). (c) 3D image of terrace structure of the $(PT_{10}T)_{45}$ film on OTS-treated wafer. (d) Terrace step profile of $(PT_{10}T)_{45}$ film on treated OTS wafer determined from topography of c); e) and f) AFM phase images of $(PT_5T)_{45}$ thin film on silicon wafer. The yellow bars and blue dotted lines stay for the individual polymer chains and their lamellae, respectively. The blue arrows indicate the average length of polymer chain. The black arrows indicate the interlamellar distance of the lamello-columnar local organization.

lamellar sublattice and the (200) reflection of the columnar sublattice actually correspond to the same periodicity in the intertwined lamello-columnar lattice. Moreover, the stacking of the triphenylenes into columns gives rise to a half diffuse reflection (h_T) located at about 0.355 nm with a correlation length of about 6 nm (Scherrer formula). In the ED pattern, this reflection is oriented along the polythiophene backbone direction, indicating that the stacking of the triphenylenes fluctuates around a preferential direction coinciding with the polymer chain direction.

The observation of the lamellar periodicity by TEM and ED in a normal incidence configuration implies that polythiophene stacks, triphenenylene columns and aliphatic medium alternate in the substrate plane. In consequence, both the scattering due to the stacking of polythiophenes (h_{PT}) and the fundamental reflections specific of the columnar sublattice are inaccessible in the configuration of TEM. The "h_{PT}" scattering is anyway very weak or extinct, as shown by its absence in the powder patterns of $(PT_{10}T)_{158}$, the overlapping with the h_T scattering having been excluded by comparison with a reference P3HT recorded versus temperature (h_{PT} = 3.80 + 0.03 Å between room temperature and 150 °C, Figure S10, Supporting Information). This means that the stacking of the polythiophene backbones cannot be very regular, in spite of the several sublayers' alternations within the well-defined layers. The reflections specific of the columnar sublattice area is obviously present in the powder patterns and should be observable in thin films by using a grazing-incidence configuration. Thus, the pattern, acquired on a synchrotron GISAXS line with the X-ray beam parallel to the polymer backbone (Figures 8 and S13), logically contains on the equator the lamellar orders evidenced by TEM/ED, but also on the meridian a reflection revealing the stacking of rows of triphenylene columns. The enlarged width of this additional reflection would correspond to a correlation length in the order of 200 Å, but this value is just a lower limit, as experimental causes contribute to the enlargement (angular divergence of the beam, extended sample size in the beam direction). Actually, a certain degree of structural disorder is expected, since the directional solidification occurs around 63 °C, i.e. below the annealing temperature of $(PT_{10}T)_{158}$ in the

dx.doi.org/10.1021/ma4020356 | *Macromolecules* 2014, 47, 1715−1731

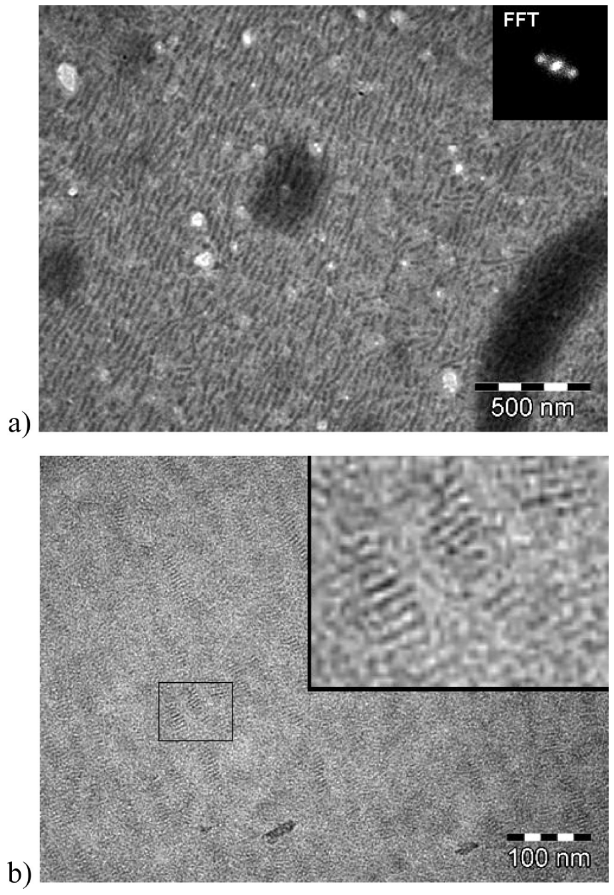

Figure 6. (a) TEM BF images of an oriented $(PT_{10}T)_{158}$ thin film, exhibiting alternated dark and bright stripes, attributed to crystalline lamellae and amorphous zones, respectively (FFT shown in inset); (b) HR-TEM image showing the substructure within crystalline lamellae, i.e., a periodic fringed pattern with a 5-nm periodicity (inset view: 4 × 4 magnification of the zone delimited by the rectangle).

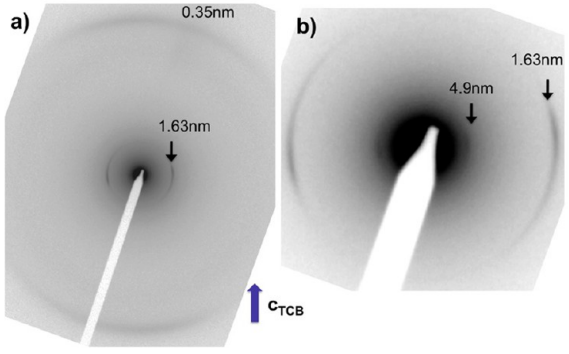

Figure 7. (a) ED pattern of an oriented $(PT_{10}T)_{158}$ thin film; (b) magnification of the small angle region. The blue arrow indicates the growth direction of TCB (c_{TCB}). The reflections at 1.63 and 4.88 nm correspond to the 1st and the 3rd lamellar orders (i.e., to the reflections (0 2) and (0 6) of the lamello-columnar lattice, Table 3).

bulk. The technique of alignment concerns the polymer backbones and therefore the layers but should not influence the columnar packing within the layers, which is not long-range correlated in the bulk at the film preparation temperature. Indeed, very similar patterns are observed in the bulk on first heating in the partially annealed sample, the lamellar order becoming long-range before the columnar order: sharp lamellar

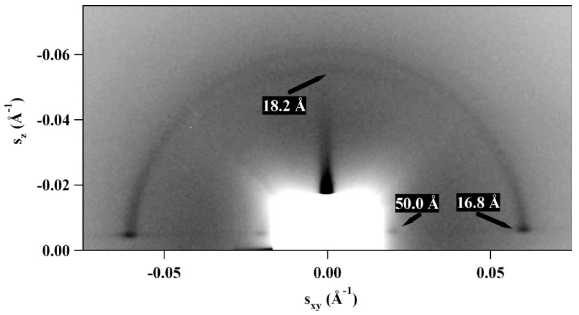

Figure 8. GISAXS pattern of an oriented $(PT_{10}T)_{158}$ thin film with the X-ray beam parallel to the backbone direction. In consistency with TEM and ED results, the 1st and the 3rd lamellar orders appear on the equator. In addition, an equatorial arced peak at 18.2 Å on the equator shows the columnar registry.

reflections coexist then with an unique diffuse reflection located at 18.2 Å ($\xi \approx 100$ Å) (Figures 8 and S13, Table 3).

DISCUSSION

Lamello-Columnar Structure of the Polymers of the $(PT_{10}T)_n$ Subseries. The completion of the "phase" transformation induces the long-range ordered columnar and lamellar sublattices, which are the same for the three polymers $(PT_{10}T)_n$, the location and intensity ratios of the reflections in the patterns being nearly identical (Figures 1, S7, S8). This observation is a logical consequence of the medium-range correlated organization in the common direction of polymer backbones and columns: the associated correlation length ($\xi_T \approx 60-70$ Å) is close to the theoretical backbone length of the shortest polymer ($(PT_{10}T)_{15}$), but substantially below for the other polymers, and a further increase of DP_n should then not any more influence the organization.

The closeness of one of the columnar first order periodicities to the third lamellar order allows suggesting the lamello-columnar organization, which consists in a bidimensional lattice with a periodicity of three rows of columns ($N_{Trow} = 3$) along the coincidence direction (e.g., lattice tripling). The symmetry turns out to be rectangular, the *a*-lattice parameter being assigned to the direction of the normal to the lamellae and the *b*-parameter, to the direction of the rows. As shown hereafter the lattice includes two lamellae and two columns per row, corresponding to $N_T = 12$ columns and $N_{PT} = 12$ backbones per lattice (Table 3, Figure 9a). In the direction perpendicular to the lattice plane, a periodicity of 2 polymer repetition units is considered because of the herringbone conformation of backbones. This defines an elemental cell containing $Z = 24$ repetition units whose volume is estimated to 1380 ± 80 Å^3 from partial volume data ($\rho = 1.08 \pm 0.06$ g/cm^3); a cell periodicity perpendicular to the lattice, $h = 8.2 \pm 0.5$ Å (caption of Table 3), is then deduced from the ratio of the cell volume V ($33 \pm 2 \times 10^3$ Å^3) and of the lattice cross-section area ($S = 4.04 \times 10^2$ Å^2). This value is actually close to the theoretical periodicity along the polymeric backbone ($2 \times l_{PT} \approx 7.70$ Å[13b,32]), which would be the one for perfectly registered backbones of infinite length and orthogonal to the lattice plane. The discrepancy with the thickness of two stacked triphenylene rings is slightly larger ($2 \times h_T \approx 7.10$ Å) and must be compensated by fluctuations in the ring orientation, as suggested by ED patterns, or by other mechanisms contributing to the disorder in the structure.

dx.doi.org/10.1021/ma4020356 | Macromolecules 2014, 47, 1715−1731

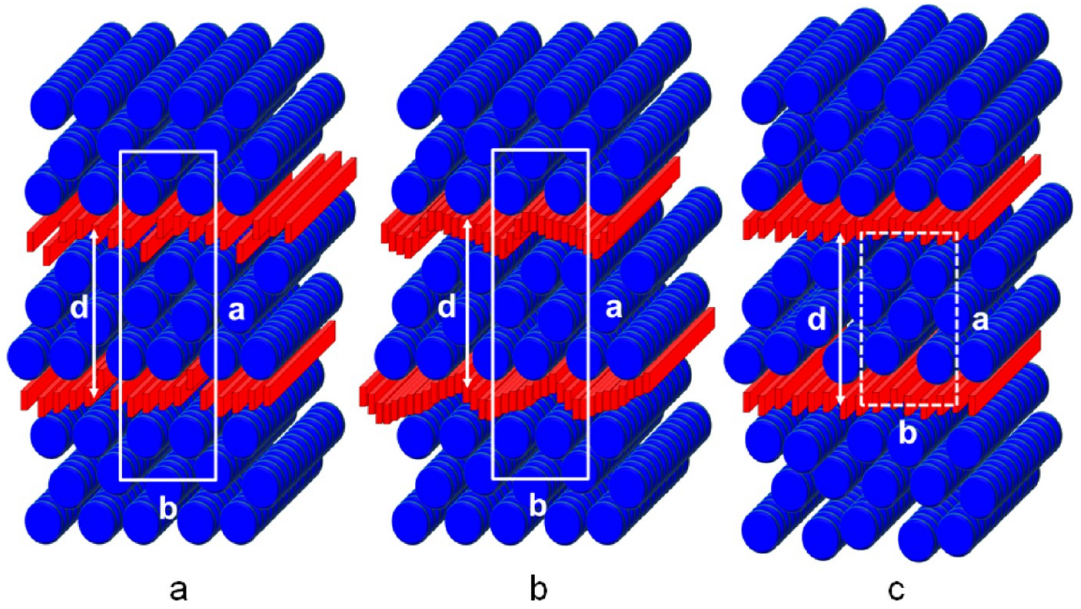

Figure 9. Schematic views of the supramolecular organization of (a) $(\mathbf{PT_{10}T})_n$ polymers in the $LamCol_R$ phase, (b) $(\mathbf{PBTT})_{21}$ copolymer in the $LamCol_R$ phase, and (c) $(\mathbf{PT_{15}T})_{45}$ polymer in the Lam_{Col} phase. Blue discs represent the triphenylene columns and red boards, the polymer backbones; the molten aliphatic parts fill the empty spaces. Column and backbone axes are perpendicular to the lattice plane. *d* is the lamellar periodicity; *a* and *b* are the parameters of the rectangular lattice delimited by the thick white lines ($LamCol_R$ phase) or of the average repetition unit of the local organization within lamellae visualized by the dashed lines (Lam_{Col} phase).

The segregation in alternating sublayers of backbones and columns separated from molten chains takes place by compromising the constraints coming from the different bulkiness of the polymers and pending groups, from the short interconnection through the aliphatic spacer and from the conformation of the polymer. For the description of this aspect of the mesophase organization, additional geometric parameters are needed, in particular the ″packing area″ A, which is defined as the projection area of the unit cell in the plane of lamellae ($A = 12V_M/d \approx 327$ Å^2). Another useful parameter is the section of triphenylene columns parallel to the columnar axis $2\sigma_{Tch}$, which is deduced from the volume fraction of hexa(pentyl)-triphenylene in the polymer ($f_{Tch} \approx 0.86$) and from the lattice area per column S/N_T, by considering an equal repartition of the chains around the cores: the distance between columns a_{Tch} would then be the same as in a hexagonal columnar phase ($a_{Tch} = [f_{Tch} \times S/N_T \times 2/\sqrt{3}]^{0.5} = 18.3$ Å), determining $2\sigma_{Tch}$ ($2\sigma_{Tch} = h \times a_{Tch} \approx 150$ Å^2). The packing area is close to the section of 2 columns, in consistency with the triple row organization deduced from X-ray patterns, the small difference between molecular areas being attributed to experimental errors, to a dissymmetric repartition of aliphatic tails around the columnar cores and to the volume contribution of the spacers connecting the polymers to the inner row of columns.

The six polymers constituting a single sublayer would cover a minimum surface $6\sigma_{PT}$ if they were stacked with the backbone plane parallel to the layer normal ($6\sigma_{PT} = 6 \times h_{PT} \times 2 \times l_{PT} = 176$ Å^2). A contrario, the much larger packing area reveals that backbones are considerably tilted in the lattice plane or less tilted but partially mixed with the molten aliphatic tails filling gaps in the backbone sublayer. Whatever the mechanisms involved in adapting the various molecular areas, the discrepancy with $6\sigma_{PT}$ prevents the regular stacking of backbones, as confirmed by the absence of the h_{PT} scattering in SAXS powder patterns (vide infra). A more favorable sublayer organization with better segregated backbones would exhibit a smaller packing area and therefore lead to an increased number of rows in the triphenylene sublayers, which is hindered by the limited length of the aliphatic spacer. Thus, in the triple row organization the constraint of the spacer can be evaluated from the shortest distance separating columnar cores and backbones in the case of an equal repartition of the molten aliphatic chains around the columnar cores. This shortest distance would then be of about 19 Å, if the columnar cores are assimilated to cylinders of 10 Å diameter (according to the section deduced from the estimated volume fractions). However, the decyl spacers impose a maximum distance between backbones and triphenylenes of only 14 Å and therefore pull the columns of the inner row within the aliphatic periphery of the outer rows. Consequently columns are alternatively up and down shifted in the inner row and likely wide and narrow spaced in the outer rows, resulting in the double-column periodicity along the *b*-axis. Corollary, backbones connected to a column of an inner row are also shifted toward this inner row. Because of the herringbone conformation of the polymers, half of the pending groups of this polymer must then come from the outer row of the next triphenylene sublayer, forcing outer and inner rows of neighboring sublayers to face and generating the two layer periodicity along the *a*-axis. A schematic representation of this packing model with *p2gg*[34] symmetry is displayed in Figure 9a.

Effects of the Bulkiness and Spacer Chain-Lengths. *Copolymers.* Three main molecular features appear to constrain the molecular packing in this particular lamello-columnar phase: (i) the different bulkiness of the triphenylene and of the polythiophene moieties; (ii) the limited spacer length and (iii) the intrinsic semicrystalline structure imposed by the P3HT backbone. Removing a fraction of the triphenylene rings connected to the polymer permits the tuning of the respective bulkiness between polymers and pending groups. As described above, different copolymers alternating alkyl and triphenylene side groups were prepared

dx.doi.org/10.1021/ma4020356 | *Macromolecules* 2014, 47, 1715−1731

with different thiophene/triphenylene ratios. Thus, as this ratio was raised (1:1 → 2:1), SAXS patterns of the alternated copolymer $(\mathbf{PBTT})_{21}$ did not evidence any change for the $LamCol_R$ mesophase organization, for which very similar geometrical parameters were retrieved (a slight 2% elongation of the lattice along the a-direction being solely noticed). The main differences with respect to the homopolymers consist in the appearance, next to the h_T scattering at 3.56 Å, of an additional scattering at 3.81 Å, attributed to h_{PT}, and in the extension of the visible lamellar order series up to the eighth order (Table 3). These results attest the now regular stacking of backbones, leading to a much improved segregation in sublayers with sharper interfaces and then to a reinforced stability of the organization, as confirmed by the extension of the mesophase range to higher temperature. Thus, using the same methodology as above (partial molecular volumes and transverse cross sections of molecular segments), the unit cell now contains $N_{PT} = Z = 24$ backbones for a slightly enlarged cell periodicity perpendicular to the lattice ($h = 10.0 \pm 0.7$ Å) and packing area ($A = 12V_M/d = 396 \pm 30$ Å^2). The minimum surface covered by the 12 polymers constituting a single sublayer $12\sigma_{PT}$ ($12\sigma_{PT} = 12 \times h_{PT} \times 2 \times l_{PT} = 352$ Å^2) is now close to A, allowing a regular stacking with the backbone plane close to the layer normal, in consistency with experimental observations (Figure 9b). Moreover, because of the herringbone conformation combined to the alternated structure, all pending groups should come from the same side of the polymer and the registry of successive triphenylene layers does now occur with the alternated up and down stacking of backbones. The significant difference between h, $2 \times l_{PT}$ (≈ 7.70 Å) and $2 \times h_T$ (≈ 7.12 Å) reflects the disorder in the packing, in relation with the reduced correlation length of the columnar piling and the relative shortening of the polymer (vide infra). Remarkably, all these changes in the polythiophene sublayer do not influence significantly the lattice geometry and the triple-row organization within the triphenylene sublayer.

Increasing this ratio (to 3:1 and 4:1) led to the complete suppression of the mesomorphism for the other two copolymers, $(\mathbf{PTTT})_{14}$, and $(\mathbf{PQTT})_9$. If the $LamCol_R$ mesophase would have been maintained for the alternated copolymer $(\mathbf{PTTT})_{14}$, the number of backbones per sublayer would have reached 18 for a minimum surface $18\sigma_{PT}$ ($18\sigma_{PT} = 18 \times h_{PT} \times 2 \times l_{PT} = 528$ Å^2) exceeding substantially the packing areas of the triple row organizations described above. One may have expected that the packing within the triphenylene sublayer would then change for a double-row organization realizing the adaptation of molecular areas. In practice, the material does not show any type of mesophase organization and is amorphous at all temperature, exhibiting exclusively a glass transition close to room temperature. The SAXS patterns confirm the absence of long-range order, as they contain a single broad small-angle scattering at about 17 Å which corresponds to average intermolecular distances; trivially lateral distances between chains and other moieties give rise to a broad wide-angle scattering with a maximum located at about 4.3 Å. It should be mentioned that the h_T scattering is not visible in the patterns, indicating that triphenylene rings do not pile regularly. This observation may be directly related to the absence of mesophase organization: because of the herringbone conformation, the periodicity along the polymer chain has now reached $6 \times l_{PT}$ (= 23 Å). On each side of the backbone, two successive pending groups bearing triphenylene rings are now separated by two pending groups constituted by octyl chains, which logically hinder the stacking of the rings. The influence of the triphenylene logically further declines for **PQTT** giving rise to a room temperature molecular organization that comes down to alternating sublayers of backbones and pendent groups. Indeed the molecular area ($S \approx 62$ Å^2) deduced from layer spacing ($d \approx 36$ Å) and repeat unit volume ($V_M \approx 2240$ Å^3) hardly exceeds the minimum section of well stacked polythiophenes ($4\sigma_{PT} \approx 58$ Å^2), confirming the evolution toward a lamellar structure resembling to P3HT. In consistency with the reduced intensity of the first lamellar order, pendent groups bearing and devoid of triphenylene form intermediate strata of increased electronic density roughly in the middle of pendent group sublayers. These strongly disorganized strata might then cause bending and other deformations of layers, and delay the appearance of the orientational long-range order despite well segregated polythiophene sublayers.

Thus, to summarize, the variation of the thiophene/triphenylene ratio showed that the triple row organization persists with loosely packed and with close stacked backbones (for the homopolymers and the former copolymer, respectively). Unfortunately, the mesophase properties vanish for a further expansion of the polythiophene sublayer, following concomitant structural changes.

Effect of the Spacer-Length. We next investigated the influence of the spacer-length between the **PT** backbone and the triphenylenes, suspected to play a major role in the occurrence of the $LamCol_R$ phase. Thus, for the homopolymer $(\mathbf{PT_{15}T})_{45}$, i.e. with a pentadecyl spacer, the maximum distance between backbones and triphenylenes reaches 20 Å, which is then comparable to the shortest distance separating columnar cores and backbones, in the case of an equal repartition of the molten aliphatic chains around the columnar cores (i.e., 19 Å, vide infra). In the case of $(\mathbf{PT_{10}T})_n$ polymers, the discrepancy between both distances was supposed to pull the columns of the inner row between those of the outer rows, but this constraint of limited spacer length now vanishes for the $(\mathbf{PT_{15}T})_{45}$ polymer. Surprisingly, this leads to a drastic reduction of mesophase ordering, the isotropization temperature decreasing by nearly 40 °C with respect to $(\mathbf{PT_{10}T})_{45}$ and the long-range ordered columnar sublattice being replaced by a unique half diffuse reflection located at about 18 Å. Yet the lamellar stacking is long-range and the intensity modulation in the lamellar order series reveals that the segregation in lamellae and rows is very close to the one in the $LamCol_R$ phase. Moreover, ED patterns on oriented thin films (also prepared with the DEC method) confirmed the attribution of the very strong third lamellar order and showed that the layers are still parallel to the polymer backbones (Figure S14). The only significant change of the lamellar ordering with respect to $(\mathbf{PT_{10}T})_n$ consists in a substantial increase of the thickness (by about 8 Å, i.e. 15%), which is a logical consequence of the release of the constraints due to the spacer. Thus, with the vanishing of the up and down shifts in the inner row, the same columns may be composed of triphenylene rings coming from both sides of the triple rows which may explain the apparition in the X-ray pattern of an additional diffuse scattering at twice h_T, corresponding to the dimer periodicity (h_{2T}).[35] The sharing of columns between several backbones would then contribute to the disorder in the piling and in the lateral packing of columns, but would mainly decorrelate the locations of successive triple rows. This may then be the cause of the reduction of the long-range $LamCol_R$ ordering to a lamellar

dx.doi.org/10.1021/ma4020356 | Macromolecules 2014, 47, 1715−1731

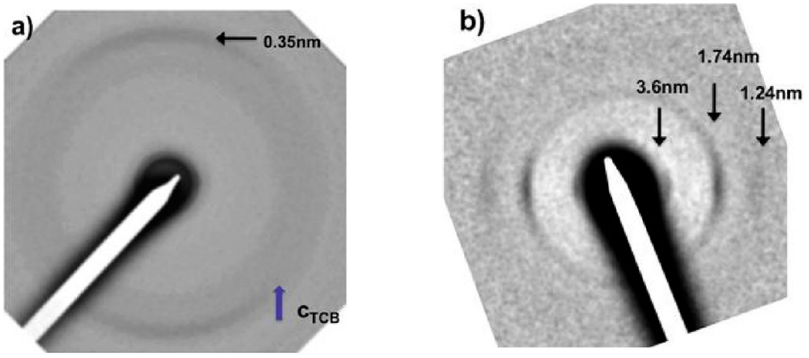

Figure 11. (a) ED pattern of oriented $(\mathbf{PT_5T})_{45}$ thin films; (b) magnification of the small angle region. The blue arrow indicates the growing direction of TCB crystals. Bows in the wide-angle region are located at about 3.49 Å and result from the stacking of triphenylene rings (h_T). The reflections centered at about 36.1, 17.4, and 12.3 Å correspond to the three first orders of the short-range correlated lamellar stacking.

phase with short-range correlated columnar registry (abbreviated as Lam_{Col}, Figure 9c).

Despite the loss of the columnar long-range ordering, the release of the spacer-length constraints preserves the organization in triple rows alternating with backbone sublayers. It is expected this not to remain if the spacer is shortened to pentyl, i.e. to the length of the tails in the periphery of columns. Indeed, $(\mathbf{PT_5T})_n$ polymers exhibit another type of mesophase, stable over an extended temperature range (Table 4). On first heating, the DSC traces contain several undefined signals corresponding likely to the annealing and to the gradual fluidification evidenced by POM, leading to fluid textures typical of a uniaxial nematic phase ca. 20 °C below the isotropization temperature (vide supra). These textures are then kept on cooling and on further heating runs with a gradual variation of the viscosity, while only the signals of the isotropization and of the glass transition are visible in DSC traces. X-ray patterns do not change significantly in the mesophase range and are even very close to the patterns in the pristine state. The main difference concerns the h_T scattering, which is not detected on the first heat until the glass transition is crossed and which vanishes then again at the isotropization temperature. In the small-angle region, a scattering with a maximum, located at 17 to 18 Å, is observed throughout the mesophase domain up in the isotropic state. Indeed, the absence of any sharp reflections in the mesophase confirms its assignment to a nematic phase, but the careful analysis of the scatterings shows that it can be decomposed into several diffuse reflections of unequal width and intensity (Figures 3 and S9, inset views from 4° to 8°). On the first heat, the analysis is ambiguous, probably because of small structural changes occurring gradually with the fluidification noticed by POM, but on cooling the composition of the scattering is clear and surprisingly constant in the whole nematic range and moreover identical for both polymers.

Thus, these signals consist in 4 broadened lamellar orders overlapping a more diffuse reflection D_T related to the spacing of columns (Table 4). The correlation lengths associated with these reflections and to the h_T scattering correspond roughly to 3 lamellae, 3 columns and about 11 rings piled into columns. This suggests classifying this mesophase among the columnar nematics, but with an unconventional lamello-columnar local positional ordering (thereafter designated as N_{LamCol}).

Oriented patterns might help to describe the local positional ordering and both samples were slowly cooled down from the isotropic state in a 1.0 T home-built magnetic oven equipping a specific SAXS line, but patterns did not evidence any alignment of the sample. Fortunately, the preparation of oriented thin films by DEC was finally successful for the $(\mathbf{PT_5T})_{45}$ polymer. ED patterns on these oriented thin films contain the lamellar orders and the h_T scattering bows in perpendicular directions, the latter direction coinciding roughly with that of the polymer chains (Figure 11). The segregation type is therefore similar to the one existing in the $LamCol_R$ phase, except that the lamellar periodicity is now shrunken by about 1/3; the most intense reflection in the series, which is now the second order, confirms the expected organization change from triple to double rows of columns. In consequence, the packing area drops by about 50% and spaces backbones, which are hence buried in the periphery of interconnected columns. This suggests a new view of the organization, based on the arrangement in disorganized layers of dimers, constituted by the whole of two columns and the interconnecting backbones (Figure 12). In the absence of registry, correlations between successive layers, the D_T scattering just reflects the lateral distance between dimers. The layering is short-range correlated but the sublayer interfaces are sharp, as shown by the presence of four lamellar

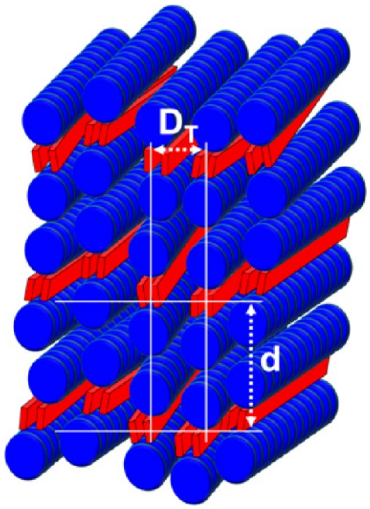

Figure 12. Schematic view of the local positional organization with the N_{LamCol} phase of $(\mathbf{PT_5T})_n$ polymers. Blue discs represent the triphenylene columns and red boards, the polymer backbones. Molten aliphatic parts fill empty spaces. Column and backbone axes are perpendicular to the sheet plane. d and D_T are the average distances between the dimers of columns and backbones.

dx.doi.org/10.1021/ma4020356 | *Macromolecules* 2014, 47, 1715−1731

orders, with intensity ratios almost reproducing the sequence of high- and low-electronic density segments in the dimers. This means that the dimers are well confined in regularly stacked but strongly bent layers, likely in relation with their large size hampering their diffusion between layers. Within nematic domains these bent layers adopt all possible orientations and the polythiophenes appear macroscopically as a uniform decoration of the interfaces between columns, whose common preferential alignment defines the nematic director. The influence of the polymer decoration on the average structure thus resembles to the swelling of the aliphatic periphery with hydrocarbon solvents that also reduces columnar long-range positional ordering to nematic columnar.[36] The polymer however confers its intrinsic properties to the material, explaining in particular the high viscosity and the freezing of the texture at low temperature, due to the approach and the crossing of the glass transition.

CONCLUSIONS

In order to completely elucidate the structure of the unconventional lamello-columnar mesophase recently discovered in regioregular triphenylene-functionalized polythiophenes, we synthesized and studied the thermal and self-organization behaviors of two series of intricate polymeric systems associating the shape-persistent regioregular poly(3-alkylthiophene) backbone with laterally pending mesogenic triphenylenes. In the homopolymer series, the length of the polymer backbones and the length of the aliphatic spacer between the polymeric backbone and the discotic side groups were systematically varied, whereas the thiophene/triphenylene ratio (i.e., the degree of polymer lateral substitution) was varied in the copolymer series. The precise structure of the lamello-columnar mesophase was elucidated principally by resorting to oriented thin film techniques developed for π-conjugated semicrystalline polymers, used for the first time for such LC systems. In particular, the directional epitaxial crystallization technique led to thin films with the backbones lying parallel to the substrate, from which the respective orientations between polymer backbones and triphenylene columns were investigated by TEM, ED, and GISAXS. Thus, backbones and columns turned out to be parallel to each other, in an overall lamello-columnar structure consisting in the alternation of triple rows of columns and of backbone sublayers.

The decyl spacer in $(\mathbf{PT}_{10}\mathbf{T})_n$ is hardly sufficient to link backbones to triphenylenes of intermediate rows and leads to periodic undulations of the layers and rows, at the origin of the large columnar sublattice involving two lamellae, 12 columns and 12 backbones. With longer spacers releasing these geometric constraints, the long-range correlated columnar superstructure vanishes, but the lamellae of alternating backbone layers and disorganized triple-rows subsist. With shorter spacers, triple-rows are expectedly substituted by double-rows, but both columnar and lamellar substructures get concomitantly short-range correlated in an overall cybotactic organization of macromolecule dimers. The common average orientation of the dimers remains however long-range correlated, as in a nematic phase of single molecules or columns. In this polymer series, the long-range lamello-columnar order only appears for the intermediate decyl spacer, when the three rows organization persists with geometric constraints. Presumably, the reason should be that these constrains correlate the respective positions of columns beyond the intercalated backbone layers, successive triple rows are disconnected otherwise.

Surprisingly the organization in triple rows does not evolve toward double rows when a fraction of the pending mesogens is removed through copolymerization with alkyl thiophene monomer. A copolymer realizing the perfect adequacy between the theoretical cross sections of both moieties (**PT** and **T**), and two more with even more diluted mesogens, were compared to the analogous homopolymers. While the more diluted copolymers are amorphous, the former copolymer shows the same mesophase as the homopolymers, over an extended temperature range. Even the geometrical parameters remain nearly unchanged; the only significant structural difference is the improved registry of backbones, due to the intercalation of the repeat units devoid of pending mesogens. Corollary, the long-range correlated structure of this copolymer involves the regular alternation of registered backbones and stacked discotic mesogens, consisting in two orthogonal π-stacking directions.

These optimized polymeric architectures based on two chemically different moieties constitute an interesting basis for the design of novel self-organized complex semiconducting materials. Associated with judicious side groups as for example n-type entities, we anticipate that this simple and versatile strategy for producing distinct conductive channels, could lead to a new class of supramolecular ambipolar materials, easily processable, potentially suitable for electronic and optoelectronic applications. Efforts in this direction are being encouraged.

ASSOCIATED CONTENT

Supporting Information

Synthetic schemes, experimental procedures and chemical characterizations of building blocks, monomers, and polymers, and DSC, XRD, and AFM data. This material is available free of charge via the Internet at http://pubs.acs.org.

AUTHOR INFORMATION

Corresponding Authors

*E-mail: (B.D.) bertrand.donnio@ipcms.unistra.fr.
*E-mail: (F.M.) fabrice.mathevet@upmc.fr.
*E-mail:(A.-J.A.) andre-jean.attias@upmc.fr.

Notes

The authors declare no competing financial interest.

ACKNOWLEDGMENTS

This work has been supported by the Pierre and Marie Curie University (UPMC), by the Centre National de la Recherche Scientifique (CNRS), and by the French Research National Agency (ANR) in the frame of its program in Nanosciences and Nanotechnologies (TRAMBIPOLY project ANR-08-NANO-051). D.A.I. acknowledges the Russian Ministry of Science and Education (Grant No 11G34.31.0055). GISAXS measurements were carried out at the National Synchrotron Light Source, Brookhaven National Laboratory, which is supported by the U.S. Department of Energy, Division of Materials Sciences and Division of Chemical Sciences, under Contract DE-AC02-98CH10886. The authors are grateful to Elaine DiMasi and Vesna Stanic for the excellent technical support during experiments at the X6B beamline.

REFERENCES

(1) (a) Forrest, S. R. *Nature* **2004**, *428*, 911−918. (b) Choi, M.-Y.; Kim, Y.; Ha, C.-S. *Prog. Polym. Sci.* **2008**, *33*, 581−630. (c) Wang, C.; Dong, H.; Hu, W.; Liu, Y.; Zhu, D. *Chem. Rev.* **2012**, *112*, 2208−2267.

(2) (a) Chochos, C. L.; Choulis, S. A. *Prog. Polym. Sci.* **2011**, *36*, 1326−1414. (b) Boudreault, P.-L. T.; Najari, A.; Leclerc, M. *Chem. Mater.* **2011**, *23*, 456−469.

(3) (a) McCulloch, I.; Heeney, M.; Bailey, C.; Genevicius, K.; MacDonald, I.; Shkunov, M.; Sparrowe, D.; Tierney, S.; Wagner, R.; Zhang; Michael, W.; Chabinyc, M. L.; Kline, J. R.; McGehee, M. D.; Toney, M. F. *Nat. Mater.* **2006**, *5*, 328−333. (b) Sirringhaus, H.; Brown, P. J.; Friend, R. H.; Nielsen, M. M.; Bechgaard, K.; Langeveld-Voss, B. M. W.; Spiering, A. J. H.; Janssen, R. A. J.; Meijer, E. W.; Herwig, P.; de Leeuw, D. M. *Nature* **1999**, *401*, 685−688.

(4) (a) Shirakawa, H.; Louis, E. J.; MacDiarmid, A. G.; Chiang, C. K.; Heeger, A. J. *J. Chem. Soc., Chem. Commun.* **1977**, 578−580. (b) Chiang, C. K.; Fincher, C. R.; Park, Y. W., Jr.; Heeger, A. J.; Shirakawa, H.; Louis, E. J. *Phys. Rev. Lett.* **1977**, *39*, 1098−1101.

(5) (a) Shirakawa, H. *Angew. Chem., Int. Ed.* **2001**, *40* (14), 2575−2580. (b) MacDiarmid, A. G. *Angew. Chem., Int. Ed.* **2001**, *40* (14), 2581−2590. (c) Heeger, A. J. *Angew. Chem., Int. Ed.* **2001**, *40* (14), 2591−2611.

(6) Bates, F. S.; Frederickson, G. H. *Phys. Today* **1999**, *52*, 32−38.

(7) (a) Oh, S.-Y.; Akagi, K.; Shirakawa, H.; Araya, K. *Macromolecules* **1993**, *26*, 6203−6206. (b) Jin, S.-H.; Choi, S.-J.; Ahn, W.; Cho, H.-N.; Choi, S.-K. *Macromolecules* **1993**, *26*, 1487−1492. (c) Coi, S.-K.; Lee, J.-H.; Kang, S.-J.; Jin, S.-H. *Prog. Polym. Sci.* **1997**, *22*, 693−734. (d) Lam, J. W. Y.; Tang, B. Z. *J. Polym. Sci. A Polym. Chem.* **2003**, *41*, 2607−2629. (e) Akagi, K. *Bull. Chem. Soc. Jpn.* **2007**, *80*, 649−661. (f) Akagi, K. *J. Polym. Sci. A, Polym. Chem.* **2009**, *47*, 2463−2485. (g) Liu, K.-P.; Yu, Z.-Q.; Liu, J.-H.; Chen, E.-Q. *Macromol. Chem. Phys.* **2009**, *210*, 707−716. (h) San Jose, B. A.; Akagi, K. *Polym. Chem.* **2013**, *4*, 5144−5161.

(8) (a) Sommer, M.; Lang, A. S.; Thelakkat, M. *Angew. Chem., Int. Ed.* **2008**, *47*, 7901−7904. (b) Segalman, R. A.; McCulloch, B.; Kirmayer, S.; Urban, J. J. *Macromolecules* **2009**, *42*, 9205−9216. (c) Huettner, S.; Sommer, M.; Hodgkiss, J.; Kohn, P.; Thurn-Albrecht, T.; Friend, R. H.; Steiner, U.; Thelakkat, M. *ACS Nano* **2011**, *5*, 3506−3515. (d) Ku, S.-Y.; Brady, M. A.; Treat, N. D.; Cochran, J. E.; Robb, M. J.; Kramer, E. J.; Chabinyc, M. L.; Hawker, C. J. *J. Am. Chem. Soc.* **2012**, *134*, 16040−16046.

(9) *Handbook of Liquid Crystals*; Demus, D., Goodby, J. W., Gray, G. W., Spiess, H.-W., Vill, V., Eds.; Wiley-VCH: Weinheim. Germany, 1998.

(10) (a) Hamley, I. W. *Angew. Chem., Int. Ed.* **2003**, *42*, 1692−1712. (b) Kato, T.; Mizoshita, N.; Kishimoto, K. *Angew. Chem., Int. Ed.* **2006**, *45*, 38−68. (c) Donnio, B.; Buathong, S.; Bury, I.; Guillon, D. *Chem. Soc. Rev.* **2007**, *36*, 1495−1513. (d) Tschierske, C. *Chem. Soc. Rev.* **2007**, *36*, 1930−1970. (e) Goodby, J. W.; Saez, I. M.; Cowling, S. J.; Görtz, V.; Draper, M.; Hall, A. W.; Sia, S.; Cosquer, G.; Lee, S.-E.; Raynes, E. P. *Angew. Chem., Int. Ed.* **2008**, *47*, 2754−2787. (f) Bisoyi, H. K.; Kumar, S. *Chem. Soc. Rev.* **2011**, *40*, 306−319. (g) Tschierske, C. *Top. Curr. Chem.* **2012**, *318*, 1−108. (h) Tschierske, C. *Angew. Chem., Int. Ed.* **2013**, *52*, 8828−8878.

(11) (a) Kim, D. Y.; Cho, H. N.; Kim, C. Y. *Prog. Polym. Sci.* **2000**, *25*, 1089−1139. (b) Pron, A.; Rannou, P. *Prog. Polym. Sci.* **2002**, *27*, 135−190. (c) Akcelrud, L. *Prog. Polym. Sci.* **2003**, *28*, 875−962. (d) Hoeben, F. J. M.; Jonkheijm, P.; Meijer, E. W.; Schenning, A. P. H. J. *Chem. Rev.* **2005**, *105*, 1491−1546. (e) Kirchmeyer, S.; Reuter, K. *J. Mater. Chem.* **2005**, *15*, 2077−2088. (f) Rose, A.; Tovar, J. D.; Yamaguchi, S.; Nesterov, E.; Zhu, Z.; Swager, T. M. *Philos. Trans. R. Soc. London, A* **2007**, *365*, 1589−1606. (g) Allard, S.; Forster, M.; Souharce, B.; Thiem, H.; Scherf, U. *Angew. Chem., Int. Ed.* **2008**, *47*, 4070−4098. (h) Swager, T. M. *Acc. Chem. Res.* **2008**, *41*, 1181−1189. (i) Grimsdale, A. C.; Chan, K. L.; Martin, R. E.; Jokisz, P. G.; Holmes, A. B. *Chem. Rev.* **2009**, *109*, 897−1091. (j) Mishra, A.; Ma, C.-Q.; Bäuerle, P. *Chem. Rev.* **2009**, *109*, 1141−1276. (k) Mbi Egbe, D. A.; Carbonnier, B.; Birckner, E.; Grummt, U.-W. *Prog. Polym. Sci.* **2009**, *34*, 1023−1067. (l) Liu, J.; Lam, J. W. Y.; Tang, B. Z. *Chem. Rev.* **2009**, *109*, 5799−5867. (m) Andrew, T. L.; Swager, T. M. *J. Polym. Sci., B: Polym. Phys.* **2011**, *49*, 476−498. (n) Xie, L.-H.; Yin, C.-R.; Lai, W.-Y.; Fan, Q.-L.; Huang, W. *Prog. Polym. Sci.* **2012**, *37*, 1192−1264.

(12) (a) Pron, A.; Gawrys, P.; Zagorska, M.; Djurado, D.; Demadrille, R. *Chem. Soc. Rev.* **2010**, *39*, 2577−2632. (b) Facchetti, A. *Chem. Mater.* **2011**, *23*, 733−758. (c) Biniek, L.; Schroeder, B. C.; Nielsen, C. B.; McCulloch, I. *J. Mat. Chem.* **2012**, *22*, 14803−14813. (d) Nielsen, C. B.; Turbiez, M.; McCulloch, I. *Adv. Mater.* **2013**, *25*, 1859−1880.

(13) (a) Chabinyc, M. L.; Toney, M. F. R.; Kline, J.; McCulloch, I.; Heeney, M. *J. Am. Chem. Soc.* **2007**, *129*, 3226−3237. (b) Brinkmann, M.; Wittmann, J.-C. *Adv. Mater.* **2006**, *18*, 860−863. (c) Osaka, I.; Zhang, R.; Sauvé, G.; Smilgies, D.-M.; Kowalewski, T.; McCullough, R. D. *J. Am. Chem. Soc.* **2009**, *131*, 2521−2529. (d) Tsao, H. N.; Müllen, K. *Chem. Soc. Rev.* **2010**, *39*, 2372−2386.

(14) (a) Kim, Y.; Cook, S.; Tuladhar, S. M.; Choulis, S. A.; Nelson, J.; Durrant, J. R.; Bradley, D. D. C.; Giles, M.; McCulloch, I.; Ha, C.-S.; Ree, M. *Nat. Mater.* **2006**, *5*, 197−203. (b) Osaka, I.; McCullough, R. D. *Acc. Chem. Res.* **2008**, *41*, 1202−1214. (c) Lobez, J. M.; Andrew, T. L.; Bulovic, V.; Swager, T. M. *ACSNano* **2012**, *6*, 3044−3056.

(15) (a) Hong, X. M.; Collard, D. M. *Macromolecules* **2000**, *33*, 6916−6917. (b) Li, L.; Counts, K. E.; Kurosawa, S.; Teja, A. S.; Collard, D. M. *Adv. Mater.* **2004**, *16*, 180−183.

(16) (a) Percec, V., Pugh, C. In *Side chain liquid crystal polymers*; McArdle, C. B., Ed.; Chapman and Hall: New York, 1989. (b) Finkelmann, H.; Rehage, G. *Adv. Polym. Sci.* **1984**, *60*−*61*, 99−172. (c) Shibaev, V.; Bobrovsky, A.; Boiko, N. *Prog. Polym. Sci.* **2003**, *28*, 729−836.

(17) (a) Abe, S.; Kijima, M.; Shirakawa, H. *J. Mater. Chem.* **2000**, *10*, 1509−1510. (b) Lam, J. W. Y.; Kong, X.; Dong, Y.; Cheuk, K. K. L.; Xu, K.; Tang, B. Z. *Macromolecules* **2000**, *33*, 5027−5040. (c) Ting, C.-H.; Chen, J.-T.; Hsu, C.-S. *Macromolecules* **2002**, *35*, 1180−1189. (d) Kuroda, H.; Goto, H.; Akagi, K.; Kawaguchi, A. *Macromolecules* **2002**, *35*, 1307−1313. (e) Stagnaro, P.; Conzatti, L.; Costa, G.; Gallot, B.; Valenti, B. *Polymer* **2003**, *44*, 4443−4454. (f) Goto, H.; Dai, X.; Narihiro, H.; Akagi, K. *Macromolecules* **2004**, *37*, 2353−2362. (g) Ye, C.; Xu, G.; Yu, Z.-Q.; Lam, J. W. Y.; Jang, J. H.; Peng, H.-L.; Tu, Y.-F.; Liu, Z.-F.; Jeong, K.-U.; Cheng, S. Z. D.; Chen, E.-Q.; Tang, B. Z. *J. Am. Chem. Soc.* **2005**, *127*, 7668−7669. (h) Zhou, D.; Chen, Y.; Chen, L.; Zhou, W.; He, X. *Macromolecules* **2009**, *42*, 1454−1461. (i) Peng, H.; Chen, Y.; Chen, L.; He, X.; Li, F. *J. Polym. Sci. A: Polym. Chem.* **2010**, *48*, 5679−5692. (j) San Jose, B. A.; Matsushita, S.; Moroishi, Y.; Akagi, K. *Macromolecules* **2011**, *44*, 6288−6302. (k) Jeong, Y. S.; Akagi, K. *J. Mater. Chem.* **2011**, *21*, 10472−10481. (l) Watanabe, M.; Tsuchiya, K.; Shinnai, T.; Kijima, M. *Macromolecules* **2012**, *45*, 1825−1832. (m) Yu, Z.-Q.; Lam, J. W. Y.; Zhu, C.-Z.; Chen, E.-Q.; Tang, B. Z. *Macromolecules* **2013**, *46*, 588−596.

(18) (a) Xing, C. M.; Lam, J. W. Y.; Zhao, K. Q.; Tang, B. Z. *J. Polym. Sci., Part A: Polym. Chem.* **2008**, *46*, 2960−2974. (b) Yu, Z.-Q.; Lam, J. W. Y.; Zhao, K.; Zhu, C.-Z.; Yang, S.; Lin, J.-S.; Li, B. S.; Liu, J.-H.; Chen, E.-Q.; Tang, B. Z. *Polym. Chem.* **2013**, *4*, 996−1005.

(19) (a) Percec, V.; Aqad, E.; Peterca, M.; Rudick, J. G.; Lemon, L.; Ronda, J. C.; De, B. B.; Heiney, P. A.; Meijer, E. W. *J. Am. Chem. Soc.* **2006**, *128*, 16365−16372. (b) Percec, V.; Rudick, J. G.; Peterca, M.; Aqad, E.; Imam, M. R.; Heiney, P. A. *J. Polym. Sci., A: Polym. Chem.* **2007**, *45*, 4974−4987. (c) Percec, V.; Rudick, J. G.; Peterca, M.; Heiney, P. A. *J. Am. Chem. Soc.* **2008**, *130*, 7503−7508.

(20) (a) Kumar, S. *Chem. Soc. Rev.* **2006**, *35*, 83−109. (b) Laschat, S.; Baro, A.; Steinke, N.; Giesselmann, F.; Hägele, C.; Scalia, G.; Judele, R.; Kapatsina, E.; Sauer, S.; Schreivogel, A.; Tosoni, M. *Angew. Chem., Int. Ed.* **2007**, *46*, 4832−4887. (c) Sergeyev, S.; Pisula, W.; Geerts, Y. H. *Chem. Soc. Rev.* **2007**, *36*, 1902−1929. (d) Kumar, S. *Liq. Cryst.* **2009**, *36*, 607−638. (e) Pisula, W.; Zorn, M.; Young, J. C.; Müllen, K.; Zentel, R. *Macromol. Rapid Commun.* **2009**, *30*, 1179−1202.

(21) (a) Kreuder, W.; Ringsdorf, H.; Herrmann-Schonherr, O.; Wendorff, J. H. *Angen. Chem. Int. Ed. Engl.* **1987**, *26*, 1249−1252. (b) Mahlstedt, S.; Janietz, D.; Stracke, A.; Wendorff, J. H. *Chem. Commun.* **2000**, 15−16.

(22) (a) Kouwer, P. H. J.; Pourzand, J.; Mehl, G. H. *Chem. Commun.* **2004**, 66−67. (b) Kouwer, P. H. J.; Mehl, G. H. *J. Mater. Chem.* **2009**, *19*, 1564−1575.
(23) Tanaka, D.; Ishiguro, H.; Shimizu, Y.; Uchida, K. *J. Mater. Chem.* **2012**, *22*, 25065−25071.
(24) Tahar-Djebbar, I.; Nekelson, F.; Heinrich, B.; Donnio, B.; Guillon, D.; Kreher, D.; Mathevet, F.; Attias, A.-J. *Chem. Mater.* **2011**, *23*, 4653−4656.
(25) (a) Loewe, R. S.; Khersonsky, S. M.; McCullough, R. D. *Adv. Mater.* **1999**, *11*, 250−253. (b) Loewe, R. S.; Ewbank, P. C.; Liu, J.; Zhai, L.; McCullough, R. D. *Macromolecules* **2001**, *34*, 4324−4333. (c) Zhai, L.; Pilston, R. L.; Zaiger, K. L.; Stokes, K. K.; McCullough, R. D. *Macromolecules* **2003**, *36*, 61−64.
(26) (a) McCullough, R. D.; Lowe, R. D. *J. Chem. Soc., Chem. Commun.* **1992**, *1*, 70−72. (b) Chen, T. A.; Rieke, R. D. *J. Am. Chem. Soc.* **1992**, *114*, 10087−10088.
(27) (a) Kumar, S. *Liq. Cryst.* **2004**, *31*, 1037−1059. (b) Kumar, S. *Liq. Cryst.* **2005**, *32*, 1089−1113.
(28) (a) Iraqi, A.; Crayston, J. A.; Walton, J. C. *J. Mater. Chem.* **1998**, *8*, 31−36. (b) Iraqi, A.; Pickup, D. F. *Polym. Int.* **2006**, *55*, 780−783. (c) Mohamada, D. K.; Chauhan, S. S.; Yi, H.; Cadby, A. J.; Lidzey, D. G.; Iraqi, A. *Solar Energy Mater. Solar Cells* **2011**, *95*, 1723−1730.
(29) (a) Hong, X. M.; Tyson, J. C.; Collard, D. M. *Macromolecules* **2000**, *33*, 3502−3504. (b) Wang, B.; Watt, S.; Hong, M.; Domercq, B.; Sun, R.; Kippelen, B.; Collard, D. M. *Macromolecules* **2008**, *41*, 5156−5165. (c) Benanti, T. L.; Kalaydjian, A.; Venkataraman, D. *Macromolecules* **2008**, *41*, 8312−8315.
(30) Higashi, T.; Yamasaki, N.; Utsumi, H.; Yoshida, H.; Fujii, A.; Ozaki, M. *Appl. Phys. Express* **2011**, *4* (091602), 1−3.
(31) Kajitani, K.; Onouchi, H.; Sakurai, S.-I.; Nagai, K.; Okoshi, K.; Onitsuka, K.; Yashima, E. *J. Am. Chem. Soc.* **2011**, *133*, 9156−9159.
(32) Brinkmann, M.; Rannou, P. *Adv. Funct. Mater.* **2007**, *17*, 101−108.
(33) Brinkmann, M.; Rannou, P. *Macromolecules* **2009**, *42*, 1125−1130.
(34) A detailed description of the $LamCol_R$ phase symmetry attribution is given in the Supporting Information (comment S1)
(35) Weber, P.; Guillon, D.; Skoulios, A. *Liq. Cryst.* **1991**, *9*, 369−382.
(36) Seghrouchni, R.; Skoulios, A. *J. Phys. II Fr.* **1995**, *5*, 1385−1405.